Enhanced dataset of global marine isoprene emission from biogenic and photochemical processes for the period 2001-2020

Lehui Cui[1], Yunting Xiao[1], Wei Hu[1], Lei Song[2], Yujue Wang[3], Chao Zhang[3], Pingqing Fu[1], Jialei Zhu[1]

[1]Institute of Surface-Earth System Science, School of Earth System Science, Tianjin University, Tianjin, 300072, China
5   [2]Center for Monsoon System Research, Institute of Atmospheric Physics, Chinese Academy of Sciences, Beijing, 100029, China
[3]Frontiers Science Center for Deep Ocean Multispheres and Earth System, and Key Laboratory of Marine Environment and Ecology, Ministry of Education, Ocean University of China, Qingdao 266100, China

Correspondence to: J. Zhu (zhujialei@tju.edu.cn)

10   **Abstract.** Isoprene is a crucial non-methane biogenic volatile organic compound (BVOC) that exhibits the largest emissions globally. It is chemically reactive in the atmosphere and serves as the primary source to generate of secondary organic aerosols (SOA) in terrestrial and remote marine regions. However, a comprehensive estimation of marine isoprene emissions is currently lacking. Here we built a module to present a twenty-year (2001-2020) global hourly dataset for marine isoprene emissions, including phytoplankton-generated biological emissions (BIO emissions) and photochemistry-generated emissions in the sea surface microlayer (SML emissions) based on the latest advancements in biological, physical, and chemical processes, with high spatial resolutions. Our dataset suggests the annual global marine isoprene emissions amount to 1.097 ± 0.009 Tg·yr^{-1}. Among these, the BIO emissions are 0.481 ± 0.008 Tg·yr^{-1} while SML emissions contribute 0.616 ± 0.003 Tg·yr^{-1}. The ability of this module to estimate marine isoprene emissions was evaluated through comparison with a series of observations of marine isoprene concentrations and emission fluxes. Annual total isoprene emission across tropical ocean shows a declining trend from 2001 to 2020. Most ocean regions exhibit a one-year emission period, whereas a significant intraseasonal period is found in the tropical ocean. This dataset can be employed as input for the simulation of marine SOA formation in earth system models. This work provides the foundation for further studies into the impact of the air-sea system on marine SOA formation and its climate effect. The DOI link for the dataset is
25   http://dx.doi.org/10.11888/Atmos.tpdc.300521 (Cui and Zhu, 2023).

1 Introduction

Biogenic organic volatile compounds (BVOCs), one of the most important components in the marine boundary layer (MBL), serves as an important role in marine secondary organic aerosols (SOAs) formation, particularly in

pristine remote ocean (Yu and Li, 2021). By further generating SOA, BVOCs have a potential impact on the radiation budget and cloud microphysical properties, thereby exerting a substantial influence on global climate change (Rosenfeld et al., 2014; Gantt et al., 2012). Among all the non-methane BVOCs species, isoprene exhibits a large emission and demonstrates significant atmospheric chemical reactivity in the marine environment (Yokouchi et al., 1999; Guenther et al., 2012; Novak and Bertram, 2020). Isoprene has a lifetime of approximately 10-100 days in seawater (Booge et al., 2018). Once released into the atmosphere, it rapidly reacts with OH radicals, resulting in a short atmospheric lifetime of about one hour (Kameyama et al., 2014). Within the marine boundary layer (MBL), isoprene can undergo oxidation, leading to the formation of semi-volatile organic compounds (SVOCs) and low-volatility organic compounds (LVOCs) such as methacrolein and methacrylic acid. These compounds actively participate in the generation of marine secondary organic aerosols (SOAs) (Claeys et al., 2004; Kim et al., 2017). Due to its significant emissions and capacity to contribute to SOA formation, marine isoprene plays a crucial role in aerosol generation and growth within the MBL. The estimation of marine isoprene emission is essential and serves as a fundamental aspect for future studies on marine SOAs and their climate effects (Carslaw et al., 2010). From the perspective of isoprene, it can directly generate effects once it is emitted in to the MBL, without any transport processes like terrestrial BVOCs needed.

Previous studies have estimated marine isoprene emissions using both bottom-up and top-down approaches. Bottom-up methods yielded emission estimates in the range of 0.11-1.36 Tg·yr^{-1} (Gantt et al., 2009; Arnold et al., 2009; Booge et al., 2016; Conte et al., 2020; Myriokefalitakis et al., 2010; Palmer and Shaw, 2005; Sinha et al., 2007; Luo and Yu, 2010; Kim et al., 2017; Brüggemann et al., 2018; Shaw et al., 2010), while top-down methods yielded estimates in the range of 1.90-13.15 Tg·yr^{-1} (Luo and Yu, 2010; Arnold et al., 2009). Over the past decades, numerous studies have provided estimates of phytoplankton-generated biological emissions (BIO emissions) and photochemistry-generated emissions in the sea surface microlayer (SML emissions) over the global ocean. The estimation of BIO emissions is typically derived from an empirical linear relationship established between ocean chlorophyll concentration and isoprene emissions. (Palmer and Shaw, 2005). This is because isoprene is a structural component and metabolic degradation product of various plant photosynthetic pigments such as chlorophyll and carotenoids (Hackenberg et al., 2017; Dani and Loreto, 2017; Booge et al., 2016). The empirical linear relationship can be further refined by taking into account different types of phytoplankton, which can vary in terms of their photosynthetic pigments and metabolic processes (Arnold et al., 2009; Gantt et al., 2009). Several enhancements and refinements have been incorporated into the calculation of BIO emissions. These updates include the diagnosis of the maximum depth of the euphotic zone each hour using the diffuse attenuation coefficient at 490nm (k_{490}) and hourly surface solar downward radiation (I_0).

60 The estimation of SML emissions is based on the surfactants present in the sea surface microlayer and their associated photochemical processes (Brüggemann et al., 2018; Conte et al., 2020). The sea surface microlayer (SML) acts as a flimsy interfacial layer between the marine atmosphere and the ocean. It is formed by natural surfactants produced through phytoplankton and other marine biological processes (Wurl et al., 2011). In previous studies, the quantification of surfactant enrichment in the SML was determined using net primary production (NPP),

65 which serves as an indicator of phytoplankton productivity. Previous studies utilized experimentally based parameters to describe the photochemical processes within the SML, as well as a 10-meter windspeed threshold indicating the point at which the SML starts to be torn apart (Ciuraru et al., 2015b; Brüggemann et al., 2017).

To date, estimates of global marine isoprene emissions have been derived by considering BIO and SML emissions pathways (Conte et al., 2020; Zhang and Gu, 2022). However, few long-term datasets with high spatial resolutions

70 is available for both types of emission till now. Previous estimates also encountered challenges related to data availability and unclear emission mechanisms, leading to uncertainties in the estimated emissions (Palmer and Shaw, 2005, Gantt et al., 2009, Booge et al., 2016, Brüggemann et al., 2018, Conte et al., 2020). Estimations for high latitudes are particularly lacking due to limited satellite data coverage during the winter months. Moreover, previous estimations of vertical distributions of chlorophyll and isoprene concentrations did not entirely align with

75 current observed vertical profiles in the subsurface ocean (Conte et al., 2020; Gantt et al., 2009; Zhang and Gu, 2022). The relationships between emissions and marine and meteorological factors, established based on localized phytoplankton populations, are regionally constrained and may not be applicable in all situations. These limitations led to discrepancies between observed emissions and the estimations obtained using previous methods.

Here, we generated a 0.25°×0.25° grid dataset of global marine isoprene emissions covering a twenty-year period

80 from 2001 to 2020 with an updated method combining the latest emission features and state-of-the-art influencing factors. Two distinct types of emissions, BIO emissions and SML emissions, were calculated by satellite-derived monthly ocean chlorophyll concentration data from MODIS and ERA5 hourly meteorological reanalysis separately. The BIO emission is derived by the correlations between isoprene production and marine chlorophyll concentration, while the SML emission is determined by the surfactant in the sea micro-layer and windspeed. The availability and

85 uncertainty of the dataset are discussed through the comparations with observed isoprene concentration and a series of sensitivity tests. Our dataset can be used as input data for climate or atmospheric chemistry models. The module also can be coupled with the earth system model to calculate marine isoprene emissions online.

The subsequent section (Sect. 2) elucidates the methods and factors employed in our estimation of marine isoprene emissions. Our results are compared with previous isoprene emission inventories and some field observations in

90 Sect. 3. The characteristics of the marine isoprene emission are analysed in the Sect. 4. Sect. 5 provides information on our dataset and data availability. Sect. 6 is the summary.

2 Methods

2.1 Input data

Twenty years (2001-2020) monthly average chlorophyll concentration data at 9 km resolution and 490 nm
95 downwelling radiative flux diffuse attenuation coefficient data with the same spatial resolution were obtained from MODIS Level 3 product in the National Aeronautics and Space Administration (NASA)'s Ocean Color Web (https://oceancolor.gsfc.nasa.gov). These two datasets were averaged into grids with a resolution of 0.25°×0.25° to fit the fifth generation European Centre for Medium-Range Weather Forecasts (ECMWF) atmospheric reanalysis (ERA5) dataset used in this study (Hersbach et al., 2023). The ERA-5 hourly average 10-meter u-wind and v-wind
100 component, 2-meter temperature, sea surface temperature and surface downwelling shortwave flux were applied in the module. Additionally, the monthly normalized water-leaving radiance at 410 nm for 2012-2020 from the National Oceanic and Atmospheric Administration (NOAA) (https://coastwatch.noaa.gov) were utilized to determine the distribution of phytoplankton types together with chlorophyll concentration. This data is at 4 km resolution and is averaged into grids with a resolution of 0.25°×0.25°. The most prevalent phytoplankton types on
105 a monthly basis from 2012 to 2020 were determined for estimations of isoprene emissions over the twenty-year period.

2.2 The BIO emission module

The phytoplankton-generated emission module was developed based on the assumption that the concentration of isoprene in the ocean remains static in each hour. This assumption implied that the net isoprene production equal
110 is approximately equal to the isoprene flux from the ocean to the MBL in hourly calculation steps. Since isoprene will be oxidized immediately once it enters the MBL because of its high chemical reactivity, the model assumes that the isoprene mixing ratio in the MBL is negligible. Typically, the lifetime of isoprene in the remote MBL is about an hour, except coastal regions where there may have abundant terrestrial isoprene transport. Due to the small isoprene mixing ratio in the remote MBL (~20 ppt, Yu et al., 2021), it is reasonable to neglect the air-to-sea flux
115 and focus on marine isoprene emission into MBL. The BIO model can be expressed by the following equations:

$$F_b = \alpha \cdot P \cdot S \tag{1}$$

where F_b (g·grid^{-1}·h^{-1}) represents the isoprene emission flux from the air-sea interface into the MBL, P (g·m^{-2}·h^{-1}) is the isoprene production rate generated by phytoplankton, S (m^2) is the grid cell area and α is a chlorophyll-based rate constant (h^{-1}) to determine the biological and chemical consumption of isoprene in seawater. Biological consumption is marine isoprene loss due to the degradation by isoprene-degrading bacteria and other microbials. Chemical consumption is caused by the photochemical processes in the surface ocean, which is calculated from reaction rate constant. The value of α is calculated by the following equation based on previous observational study (Simo et al., 2022):

$$1 - \alpha = 1 - (0.1 \times C_{chl} + 0.05) \qquad \text{(When } C_{chl} < 5.77 \text{ mg m}^{-3})$$

$$1 - \alpha = 1 - (0.1 \times 5.77 + 0.05) = 0.974 \qquad \text{(When } C_{chl} \geq 5.77 \text{ mg m}^{-3}) \qquad (2)$$

This relationship is derived from a series of observations, including coastal and open sea sites, which covered a wide ocean area. Therefore, we think it is reasonable to apply this relationship. The term $0.1 \times C_{chl}$ (d^{-1}) represents the degradation and utilization of isoprene by heterotrophic bacteria. It accounts for the observed correlation between higher bacterial activity and higher chlorophyll concentrations in the mixed layer. The second term of 0.05 represents empirical chemical consumption (d^{-1}) of isoprene (Palmer and Shaw, 2005; Booge et al., 2018). It is important to note that when the seawater chlorophyll concentration exceeds 5.77 mg·m^{-3}, α is set to a constant value of 0.974 to ensure a maximum stable biological and chemical consumption term. This approach is based on observations where the maximum seawater chlorophyll concentration was observed at 5.77 mg·m^{-3} (Simo et al., 2022). Therefore, the specific value of 0.974 was determined to account for biological and chemical consumption in nutrient-rich environments.

The isoprene production rate P, was determined by a linear relationship between chlorophyll concentration, radiation, and the diffuse attenuation coefficient at 490 nm, as well as the classification of phytoplankton types. The radiation was used to determine the term I, which was calculated as the total radiance in the euphotic layer. T_c represents the ability of isoprene production for different phytoplankton types. Four distinct types of phytoplankton (i.e. haptophytes, Prochlorococcus, Synechococcus-like cyanobacteria and diatoms) were involved, each with a different isoprene production rate defined below. These coefficients were determined in previous studies, which will be discussed in the next section. C_{chl} (mg·m^{-3}) represents the sea surface chlorophyll concentration, which was considered as a parameter within the mixed layer of each grid cell. A comprehensive explanation of the methodology used to identify the phytoplankton types will be provided in Sect. 2.3.

Here, the Eq. (3) is for isoprene production rate:

$$P = I \cdot C_{chl} \cdot T_c . \qquad (3)$$

I (m) is the integrated result of radiation in the planktonic euphotic zone, where:

$$I = 2ln(\frac{2I_0}{3600})H_{max} - k_{490} \cdot H_{max}^2 \ . \tag{4}$$

I is limited by the maximum depth H_{max} (m) (Gantt et al., 2009; Shaw et al., 2003), which is calculated by:

$$H_{max} = (-ln(\frac{2.5}{I_0}) \cdot k_{490}^{-1}) \ . \tag{5}$$

In Eq. (4)&(5), k_{490} (m^{-1}) is the diffuse attenuation coefficient of downwelling radiative flux at 490 nm, which characterize the downwelling irradiance within the water column. Finally, I_0 (J·m^{-2}) is surface solar downward radiation, for which we used hourly data here.

The aforementioned equations were utilized to estimate the hourly marine isoprene emissions originating from phytoplankton within each grid, with a spatial resolution of 0.25°×0.25°. The diurnal variation of isoprene BIO emissions was estimated based on the hourly radiation data in this module. It should be noted that isoprene BIO emissions are negligible during night time hours due to the absence of radiation, as supported by relevant observational studies (Gantt et al., 2009; Sinha et al., 2007; Hackenberg et al., 2017).

2.3 Phytoplankton types distribution

Along with various oceanological conditions of different oceans on the global scale, various dominant phytoplankton types would produce isoprene in different rates through their photosynthesis and metabolic process (Booge et al., 2018; Dani and Loreto, 2017). For instance, cyanobacteria predominantly control the isoprene emission in tropical and subtropical oceans, while diatoms exhibit higher rates at high latitudes (Dani and Loreto, 2017). Moreover, it has been observed that the larger the size of a distinct type of phytoplankton, the less likely it is to thrive in the oligotrophic region of the ocean, due to the limited specific surface area of phytoplankton cells (Alvain et al., 2008). The coefficient T_c (μmol isoprene·(g chla)$^{-1}$·h^{-1}) in the Eq. (3), which relates chlorophyll concentration to isoprene emissions, is determined by phytoplankton type. Four types of phytoplankton and their corresponding coefficients T_c in this module are 0.028 for haptophytes, 0.029 for *Prochlorococcus*, 0.032 for *Synechococcus*-like cyanobacteria and 0.042 for diatoms (Gantt et al., 2009).

The dominant phytoplankton type was determined using monthly satellite-observed normalized water-leaving radiance at 410 nm and seawater chlorophyll concentration. This classification method is based on the distinctive effects of pigments on the normalized water-leaving radiance for each phytoplankton type (Alvain et al., 2005; Alvain et al., 2008), and the details are summarized in Table 2. A simplified scheme of normalized water-leaving radiance at 410 nm is used to determine phytoplankton types for the chlorophyll range 0.04-3 mg·m^{-3} (Alvain et

al., 2005; Alvain et al., 2008). The haptophyte is a wide-spread marine producer, which dominates Chla-normalized phytoplankton standing stock in modern oceans (Liu et al., 2009). Haptophytes dominant the global ocean all year-long, with contribution varies from 45% to 70% depending on the seasons (Alvain et al., 2005). Because of its small cell volume with relatively large surface extent, this species especially dominant the oligotrophic waters. Therefore, we decided to use the coefficient of 0.028 for haptophyte in the oligotrophic waters where Chla concentration lower 0.04 mg·m^{-3} and area with missing value as suggested in Alvain (2005). Conversely, the chlorophyll concentration is greater than 3 mg·m^{-3} in many coastal areas with sufficient nutrients. The normalized water-leaving radiance data are always missing due to turbid water bodies inshore in the coastal areas, which leads to underestimated isoprene BIO emission there. Based on previous observational studies in the East China Sea, which is a typical coastal region, it was determined that the dominant phytoplankton type is a combination of 50 % diatoms and 50 % haptophytes in the grids with chlorophyll concentrations greater than 3 mg·m^{-3} (Guo et al., 2014; Li et al., 2018; Liu et al., 2016).

Table 1: Scheme of phytoplankton types and classification method.

Chlorophyll Concentration (mg m^{-3})	Normalized Water-leaving Radiation		Types	Factors (T_c)
<0.04			other type	0.028
	<0.4		other type	0.028
		0.4-0.8	haptophytes	0.028
		0.8-1.0	*Synechococcus*-like cyanobacteria	0.032
0.04-3	0.4-2.4	1.0-1.3	*Prochlorococcus*	0.029
		1.3-2.4	diatoms	0.042
	>2.4		other type	0.028
>3			50 % haptophytes+ 50 % diatoms	0.035

190 Figure 1 illustrates the monthly global distribution of marine phytoplankton types. Note that the large range of other type in the polar regions is caused by the limitations of satellite-derived data. In these polar regions, there are frequent missing values in satellite observations due to the low radiation levels during the winter months, which may lead to uncertainty regarding the phytoplankton types and BIO emissions in high-latitude regions. However, the impact of missing data in polar and subpolar regions is relatively limited, because previous studies indicated

195 that isoprene is mostly emitted in the tropical and subtropical oceans in a trade-off relationship with dimethyl sulfide (DMS) (Dani and Loreto, 2017), which is also shown in our dataset. Therefore, despite the challenges posed by missing data in polar and subpolar regions, the overall estimation of global isoprene emissions is minimally affected when using other phytoplankton types in these areas. It is also found that the other type appears in the subtropic ocean, which is generally due to the low nutrient level there resulting in the chlorophyll concentrations

200 lower than 0.04 mg·m^{-3}. For the oligotrophic ocean, our module cannot determine the specific phytoplankton type, but the emissions in these areas were still included in our estimation with emission factor of 0.028 according to the

dominance of the type haptophytes in the global ocean (Alvain et al., 2005). Another noticeable ocean area of Arabian Sea and Bay of Bengal also with other type, is affected by the weather condition in the summer months. We applied the interpolation method for each grid cells in these regions for the boreal summer emissions. The details of the interpolation method and the improvement are discussed in Sect. 2.5.
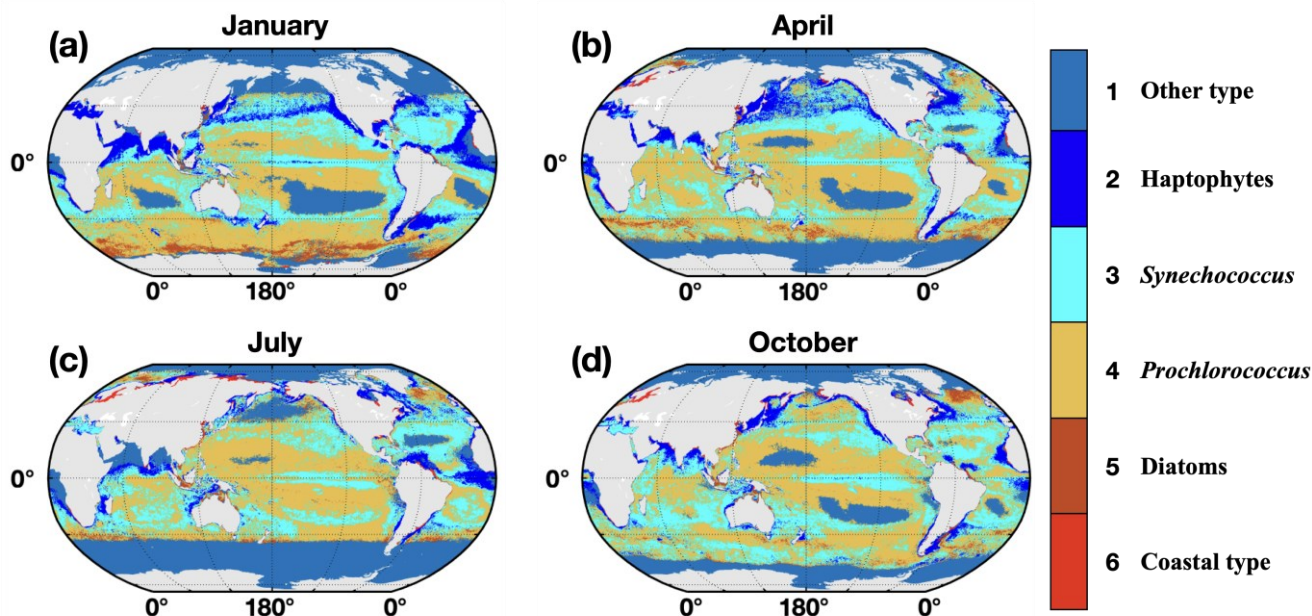
Figure 1: The spatial distribution of dominant phytoplankton types in January (a), April (b), July (c) and October (d) of 2012-2020. Six phytoplankton types are used here: 1 for other type, 2 for haptophytes, 3 for *Synechococcus*-like cyanobacteria, 4 for *Prochlorococcus*, 5 for diatoms and 6 for coastal type, which uses 50 % haptophytes + 50 % diatoms.

2.4 The SML emission module

The radiation intensity within a specific radiation band (280-400 nm) has been found as the factor determining the photochemistry-driven production and emission of isoprene according to the linear relationship between isoprene production and radiation intensity (Brüggemann et al., 2018). Here, following the parameterization of Brüggemann et al. (2018) and Conte et al. (2020), the equation below is used to estimate the marine photochemical emission of isoprene:

$$F_s = F_{lab} \times \mu_{photo} \times S \ . \tag{6}$$

Where F_s (g·grid^{-1}·h^{-1}) is the flux of isoprene emissions from the SML. F_{lab} (molecules·mW^{-1}·s^{-1}) is the flux of isoprene from marine SML and biofilm measured in previous laboratory studies (Ciuraru et al., 2015b, a; Brüggemann et al., 2017). $F_{lab} = 4.95 \times 10^7$ is used in this work, which represents the mean value within the range $(3.71 \times 10^7$-$6.19 \times 10^7)$ used by Conte, depending on the data from Brüggmann and Ciuraru (Ciuraru et al., 2015a; Brüggemann et al., 2017; Conte et al., 2020). S (m^2) is the grid cell area and μ_{photo} (mW·m^{-2}) is photochemical emission potential. The calculation of μ_{photo} is determined by Eq. (7):

$$\mu_{photo} = E_{280-400} \times F_{surf} \times k_{SML} \; . \tag{7}$$

Where $E_{280-400}$ (mW·m^{-2}) is radiation intensity, which accounts for radiation between 280 and 400 nm reaching the surface of the ocean. It is determined to be 3.535 % of the surface downward solar radiation (Conte et al., 2020)."
F_{surf} represent the different surfactant concentrations in the SML defined as a ratio given by:

$$F_{surf} = \frac{ln(c_{surf})}{ln(c_{max})} \; . \tag{8}$$

In the Eq. (8), F_{surf} accounts for a logarithmic decay of isoprene SML emissions with the decreasing surfactant concentration (Brüggemann et al., 2018). The two surfactant concentration terms, c_{surf} and c_{max}, are determined with a simplified method based on previous research, using the concentration equivalents of Triton X as the surfactant concentration in SML (Wurl et al., 2011). Here the nutrient level of the ocean is determined by the concentration of chlorophyll C_{chl} (mg·m^{-3}). The surfactant concentration reaches its maximum at $c_{max} = 663$ µg·Teq·L^{-1} , which is the mean concentration in the eutrophic waters ($C_{chl} \geq 0.4$ mg·m^{-3}) in Wurl (2011)'s experiment. A linear relationship was established to determine the surfactant concentration in the oligotrophic ocean with $C_{chl} < 0.4$ mg·m^{-3}, which is $c_{surf} = 857 \cdot C_{chl} + 320$ µg·Teq·L^{-1}. The c_{surf} approaches to 320 µg·Teq·L^{-1} while chlorophyll concentration in a low level.

The exchange velocity factor k_{SML} in Eq. (7) is calculated as the following equation (Mcgillis et al., 2004):

$$k_{SML} = \frac{8.2 + [0.014 \times w^3]}{8.2 + [0.014 \times w_{lab}^3]} , \tag{9}$$

where the parameter k_{SML} used in this study is normalized based on the work of Brüggemann et al. (2018) and Ciuraru et al. (2015a, 2015b) with $w_{lab} = 5.31 \times 10^{-2}$ m·s^{-1}, which is derived from laboratory studies (Brüggemann et al., 2018; Ciuraru et al., 2015b, a). w represents 10-meter windspeed. In addition, the SML emission is assumed to occur only when the 10-meter windspeed is smaller than 13 m·s^{-1} according to field observations (Brüggemann

et al., 2017; Brüggemann et al., 2018; Sabbaghzadeh et al., 2017). The average annual SML emission was calculated to be 0.616 Tg·yr^{-1} for the period 2001-2020, which is about 30% larger than the BIO emission.

2.5 Interpolation for missing values

Due to the influence of dust aerosols and clouds, there are regions with missing data for marine chlorophyll
250 concentration, such as the North Arabian Sea and Gulf of Guinea (30° N-30° S, 0°-120° E) and the North Pacific Subpolar Gyre (60° N-30° N, 150° E-150° W) (Alvain et al., 2005; Alvain et al., 2008). Consequently, the calculation of isoprene emissions using the aforementioned methods is not possible in these regions, leading to the underestimation of global isoprene emissions. The missing value regions primarily exist in the tropic and subtropic areas, where the seasonal variation of isoprene emission is limited. An interpolation for hourly isoprene BIO and
255 SML emission is applied during the boreal summer (June, July and August) and winter months (December, November and January) in this study. This interpolation for the missing value area based on the emission in the adjacent spring and fall months in the same grid. In the North Pacific region, missing values only occur in the summer month, with an extent comparable to interpolated regions in the tropic and subtropic areas. The same interpolation method is applied to fill the missing data and provide a basic emission status.

260 Figure 2 illustrates the interpolation process, which is an integral part of dataset establishment. This process entails utilizing the hourly isoprene emission data to calculate the monthly average diurnal variation for each grid that contains missing values. The cubic spline interpolation is then applied to determine the missing values in the summer and winter months using adjacent spring and fall emission data. The interpolated area accounts for approximately 3.1 % of the global ocean during the summer while 0.9 % during the winter. Overall, the
265 interpolation increases global isoprene emissions by 7.0 % in the summer, 3.4 % in the winter and 2.4 % for the entire year. For the comparation, the standard deviation of the twenty-year period annual marine isoprene total emission is 0.0095 Tg, which is about 0.8% of the annual total emissions. Compared to the result of the sensitivity tests, The change caused by interpolation method is smaller than most of other factors in their range of values.
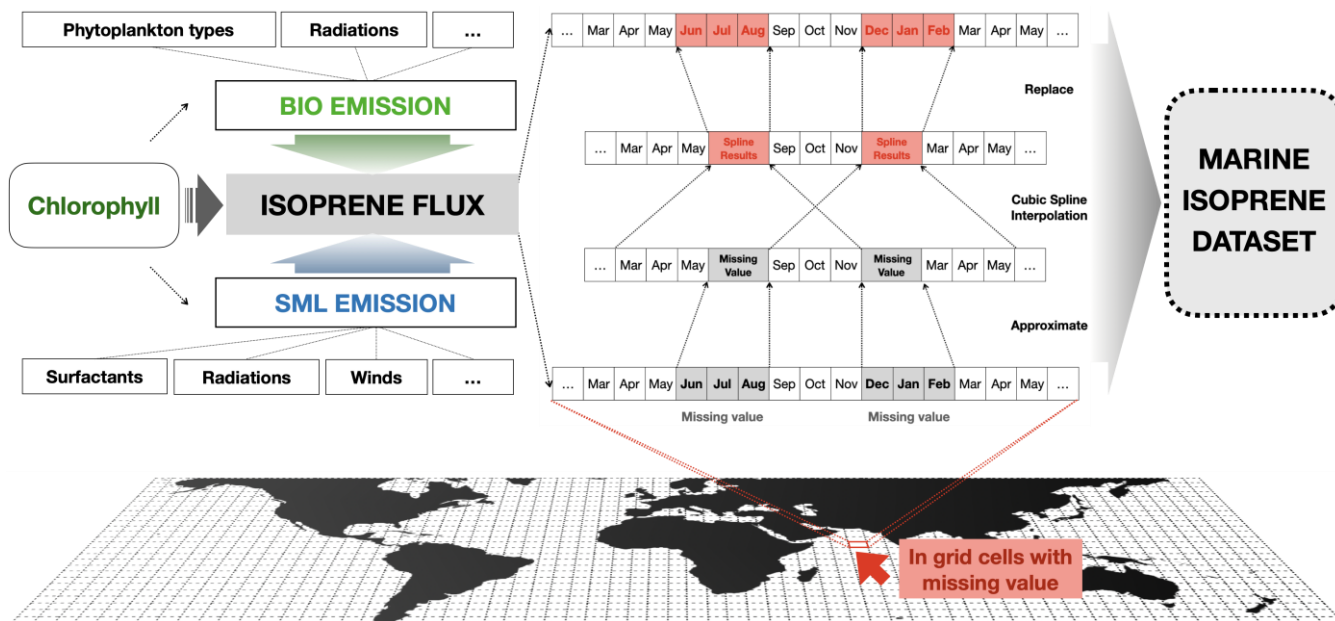
270 **Figure 2: Calculation process of the estimation and interpolation method used in our dataset. Based on chlorophyll concentration and other meteorological factors, two types of isoprene emissions were included to determine the total marine isoprene emission flux. Cubic spline interpolation was used for grid cells with missing emission values during the period of boreal summer and winter.**

3 Evaluation and comparison

275 ### 3.1 Comparison with observations

The accuracy of our method for estimating isoprene emission flux was assessed by comparing our isoprene emission dataset with previous cruise and inshore observations. Most of these results provide information on the range of isoprene concentration in the surface seawater of various regions, including Atlantic, Northern Pacific, East China Sea, Tropical Indian Ocean and Southern Ocean, while several results were derived from a single

280 sampling site with only a single value such as Tropical Pacific, Malaysia Peninsular and Mediterranean (Table 3). Furthermore, our work collected observed marine isoprene emission flux results from previous studies including four cruise researches and two inshore sites (Table 4). Most of these flux results were derived from calculations that involved the isoprene concentration in the seawater and the mixing ratio of isoprene in the marine boundary layer (method described below). Additionally, there was a floating flux chamber study conducted in the Peninsular

285 Malaysia coastal region to measure the isoprene flux directly (Uning et al., 2021) (Table 4).

The comparison of estimated isoprene emission flux and isoprene concentration in the seawater with the corresponding observations was performed in the respective regions and months. The comparison of emission

fluxes was summarized in Fig. 3. The absolute value deviations between our estimated results and the observations range from 42.3 %~45.5 % in coastal regions and from 3.64 %~54.6 % in remote oceans. Among the six comparisons, the largest deviation (54.6 %) was found in the North Atlantic region observed by Hackenberg et al. (2017) in boreal fall. However, our simulated emission flux showed a close agreement with another observation in the North Atlantic by Kim et al. (2017) with absolute value deviations of 35.4%. It is important to note that various factors, such as occasional bloom events and the inherent variability of observations, may contribute to the differences observed in the same area. The mean deviation of 33.7%, which was derived from the isoprene emission flux comparation, is smaller than most of our sensitivity results.

300   **Table 3: Observed marine isoprene concentrations in previous studies.**

Time	Location	Range (pmol · L^{-1})	References
1990 Apr	South Pacific	6.69-99.1	(Bonsang et al., 1992)
2010-2011 Dec-Jan	Southern Ocean	0.2-348	(Kameyama et al., 2014)
	Polar Northwest Pacific	1.3-31	
	Subpolar Northwest Pacific	2.2-60	
2012 Sep-Oct	Transition Water	6.4-165	(Ooki et al., 2015)
	Subtropical Indian Ocean	5.4-50	
	Tropical Indian Ocean	29-75	
2008 Nov	East Atlantic	2-157	(Booge et al., 2016)
2013 Jul	East China Sea South Yellow Sea	32.46-173.52	(Li et al., 2017)
2013 Oct-Nov	North Atlantic	21	(Kim et al., 2017)
2012 Oct-Nov	North Atlantic	8.75-63.26	
2013 Oct-Nov	North Atlantic	1.12-38.20	(Hackenberg et al., 2017)
2013 Mar	Arctic	1.96-10.57	
2013 Jul-Aug	Arctic	3.86-66.38	
2014 Jul-Aug	Indian Ocean	6.1-27.1	(Booge et al., 2018)
2014 Aug-Oct	West Pacific	15.9-33.1	(Li et al., 2019)
2018 Jul	Zenibako coastal	27.08-28	(Li et al., 2020)
	Bering Sea	21.36-67.73	
2017 Jul-Sep	Malaysia Peninsular	8.3-34.3	(Uning et al., 2021)
2018 Apr-May	Southwest UK coast	80-100	(Phillips et al., 2021)
2017 Jul	Davis Strait	59	(Wohl et al., 2022)
2019 Jul-Aug	Southern Ocean	< 54.00	(Zhou et al., 2022)
2018 Apr	Tropical Pacific	17.5	
2014 Apr-May	Mediterranean	25.1-39.0	(Simo et al., 2022)
2014 Oct-Nov	Atlantic	4.5-104.1	
2015 Jan-Feb	Southern Ocean	6.3-64.2	

Table 4: Observed marine isoprene emission flux in previous studies.

Time	Location	Range molecules $\cdot$ cm^{-2} $\cdot$ s^{-1}	Range (Daily) µg $\cdot$ m^{-2}	Methods	References
2013 Oct-Nov	North Atlantic	5.0E+7	4.84	Eddy covariance method	(Kim et al., 2017)
2017 Jul-Sep	Malaysia Peninsular	19.4E+7	18.71	Floating flux chamber TD-GC-MS	(Uning et al., 2021)
2017 Apr-May	Arabian Sea	1.5-12E+7	1.45-11.61	Seawater isoprene concentration Exchange velocity	(Tripathi et al., 2020)
2012&2013 Oct-Nov	Atlantic Ocean	0.005-34E+7	0.006-32.58		(Hackenberg et al., 2017)

Time	Location	Range nmol $\cdot$ m^{-2} $\cdot$ d^{-1}	Range (Daily) µg $\cdot$ m^{-2}	Methods	References
2001 May	Western North Pacific	161.5 (22.17-537.2)	10.98 (1.57-37.67)	Average isoprene mixing ratio	(Li et al., 2017)
2010-2011 Dec-Jan	South Ocean	181-313	12.26-21.29	Seawater isoprene concentration Exchange velocity	(Kameyama et al., 2014)
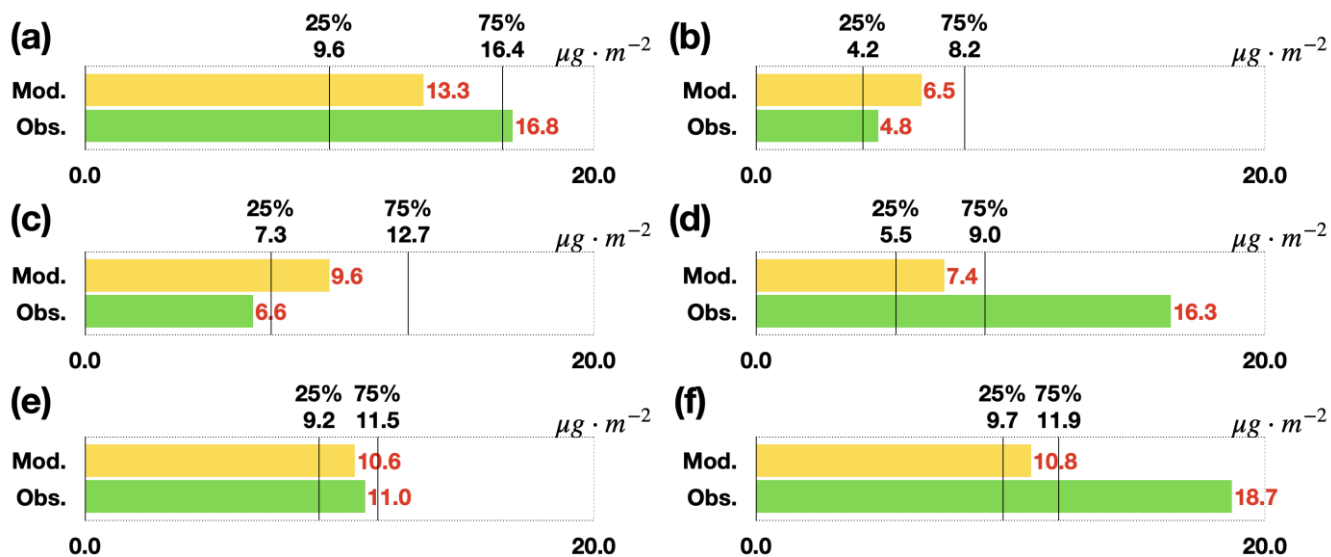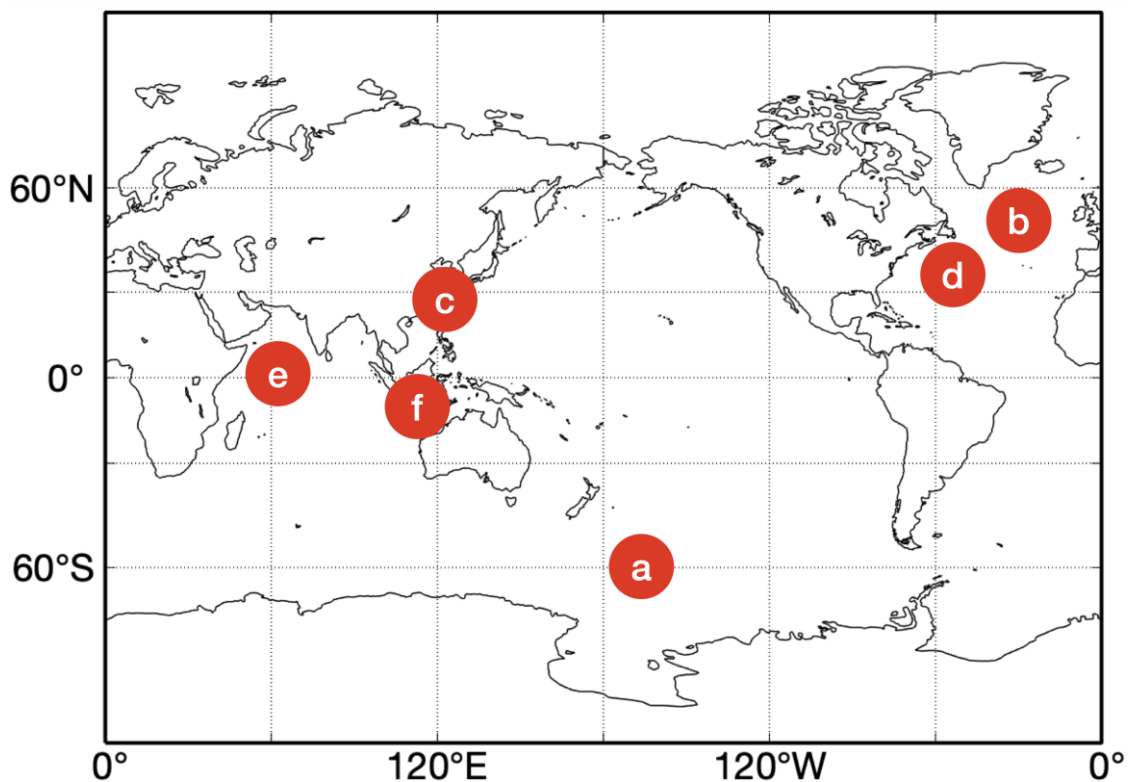
Figure 3: Comparisons between simulated isoprene emission daily fluxes (unit in μg·m⁻²) and observations. Yellow bar is daily mean isoprene emission flux in corresponding ocean regions. Two solid lines represent quartiles of the range for simulations. Green bar is the daily mean of observed emission flux. Six regions including the Southern Ocean (a) (Kameyama et al., 2014), North Atlantic (b) (Kim et al., 2017) and (d)

(Hackenberg et al., 2017), East China Sea and South Yellow Sea (c) (Li et al., 2017), Arabian Sea (e) (Tripathi et al., 2020) and Malaysia Peninsular (f) (Uning et al., 2021).

In our method, the isoprene emission flux is directly derived assuming equivalence with isoprene production, so the isoprene concentrations in seawater are not necessary to be explicitly calculated in the module described in Sect. 2. In order to compare with the observed isoprene concentration in the seawater, we calculated the seawater isoprene concentration by simulated isoprene emission flux and exchange velocity using the following equation:

$$C_{iso} = \frac{F_b + F_s}{k_{ex}} \tag{10}$$

where F_b is BIO emissions flux. F_s is SML emissions flux. k_{ex} (cm·h^{-1}) is the exchange velocity on the air-sea interface. The exchange velocity k_{ex} is determined by wind and sea surface temperature (Wanninkhof, 2014):

$$k_{ex} = \frac{0.31w^2}{\sqrt{\frac{Sc}{660}}} \tag{11}$$

where w is 10-meter windspeed. Notes that Eq. (11) is valid with w in the range of 4-15 m·s^{-1}. Sc is Schmitt number determined by sea surface temperature (Palmer and Shaw, 2005):

$$Sc = 3913 - 162.13t + 2.67t^2 - 0.012t^3 \tag{12}$$

where t is the sea surface temperature in Celsius degree. The hourly 10-meter windspeed, sea surface temperature from reanalysis data and hourly isoprene emission flux from our dataset were used to calculate sea water isoprene concentration using Eq. (11). The comparisons between simulated isoprene concentrations and observations were conducted in six regions with different latitudes and various nutrient conditions (Fig. 4). The derived isoprene concentrations from our emission flux data have range overlapping the observations in Southern Ocean, Atlantic and Eastern China Sea, while the simulated isoprene concentrations in North Pacific and tropical Indian Ocean were overestimated by 32.0 % to 48.3 % compared to observations. The exchange velocity calculated using Eq. (11) may introduce uncertainty, which could partly explain the bias between simulation and observation. The uncertainty of the method for the sea-to-air exchange process will further affect the results of marine isoprene concentrations, which is about 20% according to Wanninkhof (2014). In addition, the constant factor of 0.31 in Eq. (11) and the Schmitt number Sc determined by Eq. (12) can vary depending on ocean conditions such as solute types and sea surface temperature, which may also contribute to the bias between simulations and observations.
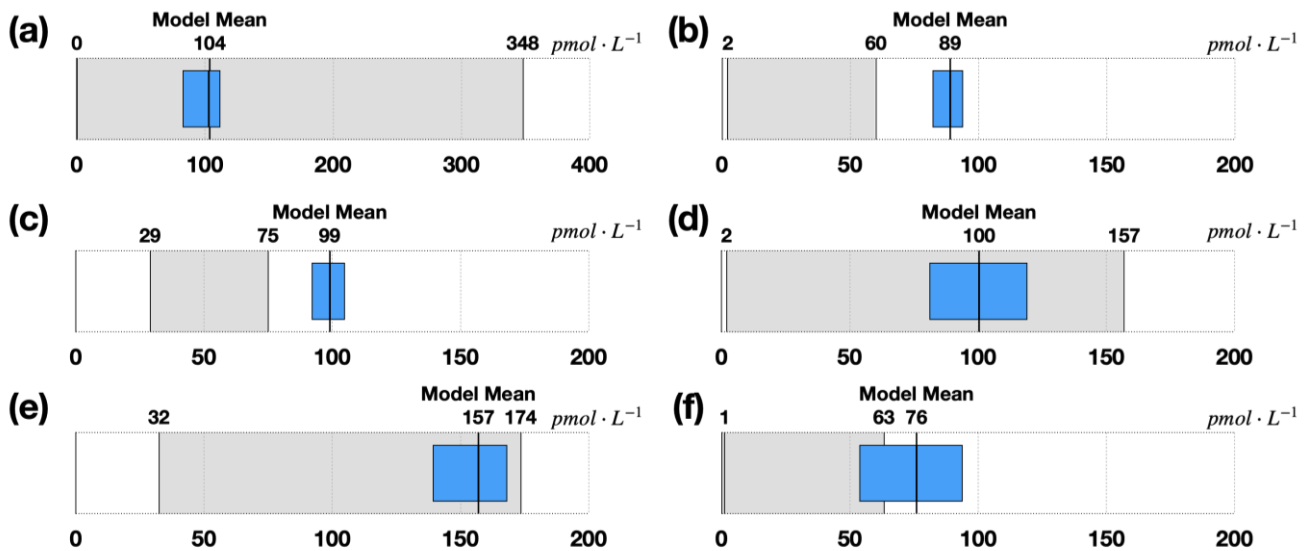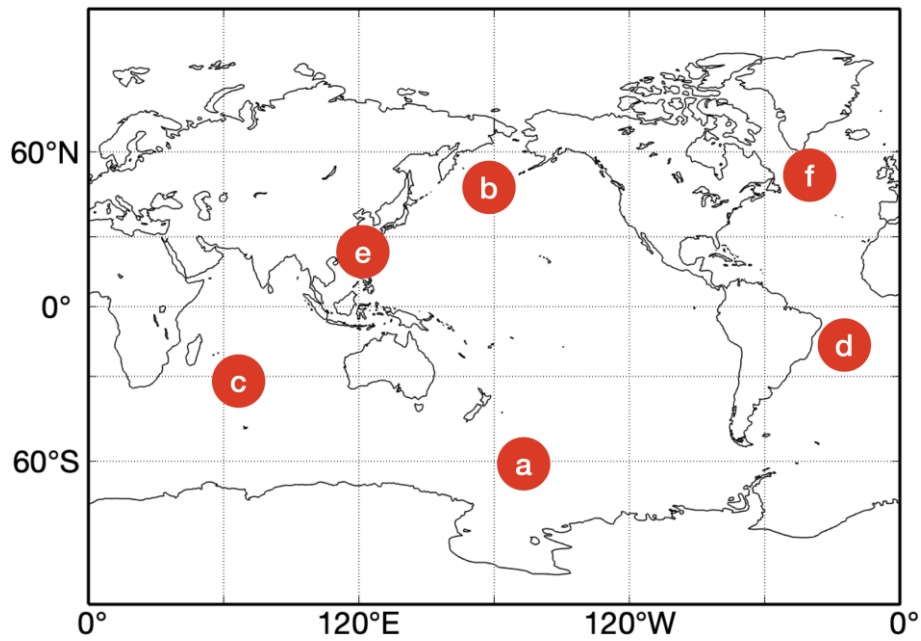
Figure 4: Comparisons between simulated isoprene concentration (unit in pmol·L⁻¹) and observations. Blue bar is the range (25-75 percentile) of simulated isoprene concentration in corresponding ocean region. The black solid line within the blue bar presents the mean of simulated isoprene concentration. Grey bar is the range of observed isoprene concentration. Six regions including the Southern Ocean (a) (Kameyama et al., 2014), Subpolar Pacific (b) (Ooki et al., 2015), Tropical Indian Ocean (c) (Ooki et al., 2015), East Atlantic (d) (Booge et al., 2016), East China Sea and South Yellow Sea (e) (Li et al., 2017) and North Atlantic (f) (Hackenberg et al., 2017).

3.2 Comparison with previous estimation results

345 The average annual isoprene emissions for the period of 2001-2020 are estimated to be 1.097 Tg·yr^{-1}, with range of 1.075-1.112 Tg·yr^{-1} using our module. Thereinto, the annual global BIO emissions range is 0.464-0.493 Tg·yr^{-1}, which corresponds to the total emissions from various types of phytoplankton. The annual global SML emissions result is in the range of 0.611-0.621 Tg·yr^{-1}, which is generated by photochemical processes in the SML. The standard deviation of the twenty-year period annual marine isoprene total emission is 0.0095 Tg, which is about 350 0.8% of the annual total emissions.

Table 2: **Marine isoprene emission estimations in previous studies.**

Compounds	Emissions Tg·yr^{-1}		Reference
	0.11	(BIO emissions)	(Palmer and Shaw, 2005)
	1.36	(BIO emissions)	(Sinha et al., 2007)
	0.79	(BIO emissions)	(Gantt et al., 2009)
	0.31	(BIO emissions)	(Arnold et al., 2009)
	1.90	(Top-down)	(Arnold et al., 2009)
	0.99	(BIO emissions)	(Myriokefalitakis et al., 2010)
	0.36	(BIO emissions)	(Luo and Yu, 2010)
Isoprene	13.15	(Top-down)	(Luo and Yu, 2010)
	0.24	(BIO emissions)	(Booge et al., 2016)
	0.65	(BIO emissions)	(Kim et al., 2017)
	1.11	(SML emissions)	(Brüggemann et al., 2018)
	0.75	(Total emissions)	(Conte et al., 2020)
	0.96	(BIO emissions)	(Li et al., 2020)
	1.10	(Total emissions)	This study

In previous studies, several model-based estimations of marine isoprene emissions were conducted, as summarized in Table 2. Most of these studies utilized a bottom-up approach, while a few employed a top-down approach. There 355 is a significant difference in the estimated isoprene emissions between these two methods. Top-down estimations generally yielding larger values compared to bottom-up estimations. This difference can be attributed, in part, to the exclusion of high-emission events and hotspots in bottom-up methods (Yu and Li, 2021). The missing values

of the source data and the unclear mechanisms of marine isoprene production, consumption and sea-air exchange all lead to the uncertainty using bottom-up method (Conte et al., 2020; Gantt et al., 2009; Hackenberg et al., 2017; Palmer and Shaw, 2005; Yu and Li, 2021). On the other hand, the limited observation datasets and insufficient spatial resolutions of input data decrease the accuracy of current top-down results (Arnold et al., 2009; Luo and Yu, 2010). Additionally, the air-sea exchange flux of marine isoprene, which is used in top-down methods, cannot be directly observed, further contributing to the uncertainty in these approaches. Furthermore, most of the available isoprene flux observations are conducted at inshore sites, which may not be suitable for estimating emissions in remote ocean areas (Simo et al., 2022). Based on the previous estimate method, our work has applied several improvements to our bottom-up method to address the existing gaps and discrepancies between top-down and bottom-up results. These improvements are discussed in detail in the next section.

3.3 Model improvements and comparisons

In our model, we implemented several ways to improve the estimation of global BIO and SML emissions compared to previous datasets. These improvements include updates to the methods and an increase in temporal and spatial resolution. The temporal resolution of the dataset was enhanced to one hour, allowing for a more detailed examination of the diurnal and seasonal variations of isoprene emissions to capture short-term changes and events that may influence emissions, which probably provides a better representation of emission dynamics. The hourly windspeed data performed better in the calculation of SML emission. The SML emission directly corresponded to the cube of windspeed (Eq. 6, 7, 9), so that the high windspeed was of large contributions. High windspeed can be captured hourly, while monthly averaging eliminates high windspeed, which results in a relative underestimation of SML emission using monthly windspeed data as input. The spatial resolution was set to 0.25°×0.25°, which is consistent with the spatial resolution of ERA5 reanalysis data. This fine spatial resolution allows for a more precise representation of the spatial distribution of isoprene emissions, particularly in coastal regions where emission patterns vary significantly. The phytoplankton types distribution scheme used in BIO emission calculation has been updated and simplified based on the normalized water-leaving radiation at 410 nm and chlorophyll concentration data, according to previous work by (Alvain et al., 2005; Alvain et al., 2008). This update helps to avoid the issue of missing phytoplankton types within a number of grid cells in coastal regions, leading to a substantial improvement in the accuracy of emission estimation in these specific areas. Moreover, a latest parameterization (in Eq. (2)) was developed to estimate the biological and chemical consumption based on observations by Simo et al. (2022) with an upper limit of 0.373 when the chlorophyll concentration was larger than 5.77 mg·m^{-3}. These

improvements help to reduce the uncertainty of BIO emission estimation and enable to examine the characteristics of BIO emission in high spatial resolution.

The estimation of SML emissions was based on the radiation, windspeed and surfactants in the sea surface
390   microlayer. Here we used chlorophyll concentration to determine the quantity of surfactants based on field measurement by Wurl et al. (2011), instead of the net primary production used in Brüggemann et al. (2018). This simplification of the model eliminates potential inconsistencies that may arise from using different datasets (chlorophyll concentration and net primary production) to describe the nutrient levels of the ocean.

395   **3.4 Data uncertainties**

The uncertainties in our model primarily presence in the parameterizations of various physical and biological and chemical processes. Since the linear relationship between isoprene emission and phytoplankton biomass is not universally applicable in all situations (Kameyama et al., 2014), a large size of measurement is required at higher spatial and temporal resolution to improve the parameterizations. Add to that, the column concentration of
400   chlorophyll was derived from satellite observation in our module with the assumption that chlorophyll is well mixed in the euphotic layer, although satellite is only able to detect the chlorophyll concentration on the surface of ocean. The isoprene productions in our model are determined by integrating over depth, taking into account the radiation levels that control the isoprene emission rate at different depths. However, previous studies indicated that the highest isoprene concentrations may occur below the surface, often coinciding with the maximum chlorophyll
405   concentrations (Conte et al., 2020; Wohl et al., 2022). As a result, uncertainty in the vertical distributions of chlorophyll and isoprene concentration under sea surface microlayer may lead to the uncertainty in the estimation of marine isoprene emission. Furthermore, previous observations detected notable VOCs emissions in the Arctic region and high-latitude South Ocean during winter (Abbatt et al., 2019; Wohl et al., 2023). These emissions may be underestimated in our model due to the limitations of satellite data. Moreover, observations have indicated that
410   isoprene production in the ocean occurs even when phytoplankton are covered by sea ice. As a result, high marine isoprene concentrations were measured in the ice edge waters and melted ponds (Wohl et al., 2022; Abbatt et al., 2019; Wohl et al., 2023). The accumulated isoprene under sea ice is emitted once the ice melts, which process was not included in our module.

Here we design several test to determine and discribe the uncertainties of this dataset. It is essential to testify and
415   quantify the possible affect factors by means of sensitivity test and to provide descriptions for the further use of the

dataset and corresponding calculation modules. The dataset has several possible source of its uncertainties., including the input reanalysis dataset, satellite data and empirical parameteraization.

The uncertainty of the annual global BIO emission is 0.443 to 0.664 $Tg·yr^{-1}$ and 0.583 to 0.655 $Tg·yr^{-1}$ for SML emission. The uncertainty of BIO emission is mainly caused by the phytoplankton types with their specific correlation correspond. These types are determined from our simplified method, with the maximum parameter used in our module for diatom and minimum parameter for haptophytes. We determined the BIO emission uncertainty range using diatom or haptophytes as the only input type. The uncertainty of SML emission is also related to the marine productivity, as the parameter of surfactant concentration is determined by chlorophyll-a concentration in our module. We split the surfactant concentration into three bins, according to the chlorophyl-a concentration. In our test for the uncertainty of SML emission, the maximum and the minimum concentration are used to determine the uncertainty range.

Our module used the dominant phytoplankton type for each month instead of higher temporal resolution due to the restriction of temporal resolution of chlorophyll-a and water leaving radiance data. We simply diagnosed the monthly phytoplankton types during period of 2012-2020. The phytoplankton types in 55 % of global grid cells were same for July in the nine-year period, while the types in 89% of the grid cells were same for over 5 of 9-year's July. The other months also have similar results. 51% grid cells are with same phytoplankton types in January, and 90% are same for over 5 of 9-year's January. For the mean percentage of the twelve months, 51% grid cells were with same phytoplankton types, and 89% are same for over 5 of 9-year. As a result, we believed it is reliable to apply the monthly dominant phytoplankton type in each grid during 2012-2020 in the estimation during all twenty years (2001-2020)."

A monthly marine isoprene emission dataset is made using the same module but with monthly input reanalysis, which also from ERA5 product. This relative low-temporal-resolution emission data was used to compared with our hourly dataset. For the global annual total emission, the mothly data result in 1.050 $Tg·yr^{-1}$, which was underestimated by 4% compared to the estimation using hourly radiation. Among this, the annual SML emission is 0.499 $Tg·yr^{-1}$, which underestimated by 19% compared to the hourly result 0.616 $Tg·yr^{-1}$. The annual BIO emission was 0.551 $Tg·yr^{-1}$, overestimated by 15% with hourly result 0.481 $Tg·yr^{-1}$. The deviation of BIO emission was mainly accounted by the accordance of the radiation data and its temporal resolution, which caused a fixed depth of euphotic layer for every month. Besides, the monthly averaged radiation ignored the influence of weather condition to radiation. The deviation of SML emission was mainly from the monthly mean windspeed data. High windspeed is eliminated by the monthly average, while the SML emission is directly corresponded with the windspeed cubed. The hourly windspeed data perform better in the calculation of SML emission. The SML

emission directly correspond to the cube of windspeed (Eq. 6, 7, 9), so that the high windspeed is of large contributions. High windspeed can be captured hourly, while monthly averaging eliminates high windspeed, which results in a relative underestimation of SML emission using monthly windspeed data as input.

450 Another input meteorological dataset is used in our module to valid the robustness of our module. We used the data from National Center for Environmental Prediction (NCEP) Global Data Assimilation System (GDAS)/FNL (final) 0.25 Degree Global Tropospheric Analyses and Forecast Grids. We derived the radiation on the ground and water surface level and wind speed at 10m for a monthly average of 2020 as input data for monthly calculations. This result (later we call it TEST result) is compared with the monthly emission data calculated from monthly ERA5

455 reanalysis, which is already discussed in the former paragraph. The TEST result turns out the global total isoprene emission is 1.132 Tg for 2020, with BIO emission of 0.588Tg and SML emission of 0.544Tg. The total emission of TEST result is of 7.8% larger then former monthly result from ERA5 reanalysis, which is 1.050 Tg·yr^{-1}. The BIO emission and SML emission in TEST result are both larger than former monthly estimations by 6.7% and 9.0%. This deviation between these two reanalysis product is obviously smaller than deviation between our dataset

460 and observed data, as well as the deviations of the result of sensitivity tests. Therefore, we think our module is valid enough and applicable to data from multiple sources.

A series of sensitivity tests were conducted for input meteorological data, input parameters and assumptions used in our module. These sensitivity tests focused on several critical input factors and parameters which may have effects on the uncertainty of the dataset. Detailed information and the results of the sensitivity test are in Table 5

465 and Table 6.

Table 5: Sensitivity test of input reanalysis data.

Emission	ERA5 Reanalysis (Tg·yr^{-1})	NCAR Reanalysis	Wind		Radiation		Chlorophyll-a Concentration	
			+50%	-50%	+50%	-50%	+50%	-50%
BIO	0.551	+6.7%	—	—	+13.6%	-21.4%	+49.9%	-49.9%
SML	0.499	+9.0%	+38.9%	-21.2%	+49.5%	-50.1%	+1.6%	-2.2%
Total	1.050	+7.8%	+18.5%	-10.1%	+31.0%	-35.0%	+26.9%	-27.2%

Table6: Sensitivity test of assumptions and parameters.

Emission	ERA5 Reanalysis (Tg·yr^{-1})	Phytoplankton Types		Surfactant		C_air		F_lab	
		All diatom: 0.042	All other: 0.028	Min: 320	Max: 663	1 ppt (Global)	1 ppt (Remote) + 20 ppt (Coastal)	Max: 6.19×10^7	Min: 3.71×10^7
BIO	0.551	+38.1%	-8.0%	—	—	-11.1%	-12.9%	—	—
SML	0.499	—	—	-5.4%	+6.4%	—	—	+25.1%	-25.1%
Total	1.050	+20.0%	-4.2%	-2.1%	+3.0%	-5.8%	-6.8%	+11.9%	-11.9%

470

The sensitivity tests are based on the monthly result of our module. For the input data, we chose radiation, 10-meter windspeed and chlorophyll-a concentration and set a 50% deviation of each factor. The results show the radiation is the most important factor for the total emission, which caused up to 35.0% deviation. The chlorophyll-a concentration is also with considerable influence to the total emissions and contribute about 27% deviation. Different influence for BIO emission and SML emission is also suggetted by the test. The radiation dominant the SML emission with about 50% of deviation, while its influence on BIO emission only up to 21.4%. On the contrary, the chlorophyll-a concentration contributes half of the deviation of BIO emission, but only about 2% for the SML emissions. This result suggests the chlorophyll-a concentration concentrates in the large value and small value. Notes that the wind speed only affect the SML emission, while the larger wind speed contribute approximately twice of the deviation as the smaller wind does. It reflected the non-linear relationship between the wind speed and SML emission.

Besides, we design several tests for the assumption and parameters used in our module, including the phytoplankton types, surfactant concentration in the sea micro-layer, fixed euphoric zone depth and the assumption for the zero isoprene mixing ratio in the marine boundary layer (MBL). Firstly we set the phytoplankton type into "all diatom" scenario and "all other" scenario. The global total emission increases 20.0% and BIO emission increase 38.1% in the "all diatom" scenario. On the other hand, the total emission decreases only 4.2%, while BIO emission decrease 8.0% using "all other" scenario. The "all other" test result in a more stable change than using diatom as the dominant phytoplankton type. This result is similar to former conclusion that the haptophytes, which with the same emission parameter as the other type, dominant a greate extent of global ocean. The surfactant concentration test show a even smaller influence on the total (-2.1% - 3.0%) and SML emission (-5.4% - 6.4%). It suggest that the SML emission is dominanted by meteorological factors rather than marine productivity. Finally, we investigate the influence of isoprene in the MBL with various mixing ratio. An observation-based coastal isoprene mixing ratio of 400 ppt is used and applied to the global ocean (Warneke et al., 2004). It turns out a 51.0% decrease of the total emission and nearly all BIO emission is surpressed. Isoprene mixing ratios under the remote ocean condition is collected from Yu's previous work (Yu et al., 2021). Here we used the mixing ratio of 20 ppt for coastal region and 1 ppt as input data and calculated global total emission. For the mixing ratio of 20 ppt in the coastal region, the total global emission decreases 6.8%, while BIO emission decreases 12.9%. For the mixing ratio of 1 ppt, the total global emission decrease 5.8%, while BIO emission decrease 11.1%. The isoprene mixing ratio in the MBL shows a strong effect on global isoprene emission. However, previous studies suggests that the high mixing ratio in the coastal area is seriously affected by the terrestrial source, especially under the specific condition that the lifetime of isoprene is equal or even larger than the terrestrial source isoprene transportation temporal scale (Warkene et al.,

2004, Booge et al., 2016). Besides, several observations suggest a minimum isoprene mixing ratio is below the detect limit range, usually smaller than 2 ppt. We believe that in the most of remote ocean with adquate oxidation radicals, isoprene is consumed very fast with a lifetime of hours (Palmer et al., 2005, Booge et al., 2016, Conte et al., 2020). The very-short lifetime of isoprene in the MBL is still approving our former assumption of zero mixing ratio of isoprene in the MBL. Besides, even though the possible isoprene mixing ratio exsists in the MBL, which is mearsure to be several ppt, it only affects a small amount of the total isoprene emission.

4 Results

4.1 Spatial and temporal distribution of marine isoprene emissions

Generally, our dataset suggests annual global marine isoprene emissions ranging from 1.075 to 1.112 $Tg \cdot yr^{-1}$ for the period 2001-2020, with an average of 1.097 $Tg \cdot yr^{-1}$ over the twenty years. Annual average global BIO emissions for the twenty-year period were 0.481 $Tg \cdot yr^{-1}$, ranging from 0.464 to 0.493 $Tg \cdot yr^{-1}$, while annual average global SML emissions was 0.616 $Tg \cdot yr^{-1}$, ranging from 0.611 to 0.621 $Tg \cdot yr^{-1}$. In the twenty-year period, the average annual emissions in the Northern Hemisphere amounted to approximately 44.9 %, whereas the Southern Hemisphere accounted for 55.1 % of the total emissions. However, the emission per unit area in NH (3.3 $mg \cdot m^{-2} \cdot yr^{-1}$) is 6.5% larger than that in SH (3.1 $mg \cdot m^{-2} \cdot yr^{-1}$) due to the larger and better nutritional status of coastal ocean areas in NH. The difference in the total emissions between two hemispheres is largest in boreal winter (Fig. 5). The emission in the boreal winter of the Southern Hemisphere contributed 17.7 % of annual global emissions in average, while the emission in the same season of the Northern Hemisphere accounted for only 8.7 %." Meanwhile, the emission per unit area in NH (0.70 $mg \cdot m^{-2}$) was still smaller than that in SH (0.85 $mg \cdot m^{-2}$) in the boreal winter. Radiation and duration of day directly dominate the seasonal variations of total emissions as well as they affect chlorophyll concentration, thereby indirectly influence the emissions. This highlights the unneglectable importance and dominance of marine isoprene emissions in the SH compared to the NH, suggesting potential environmental impacts and climate modifications associated with these emissions.
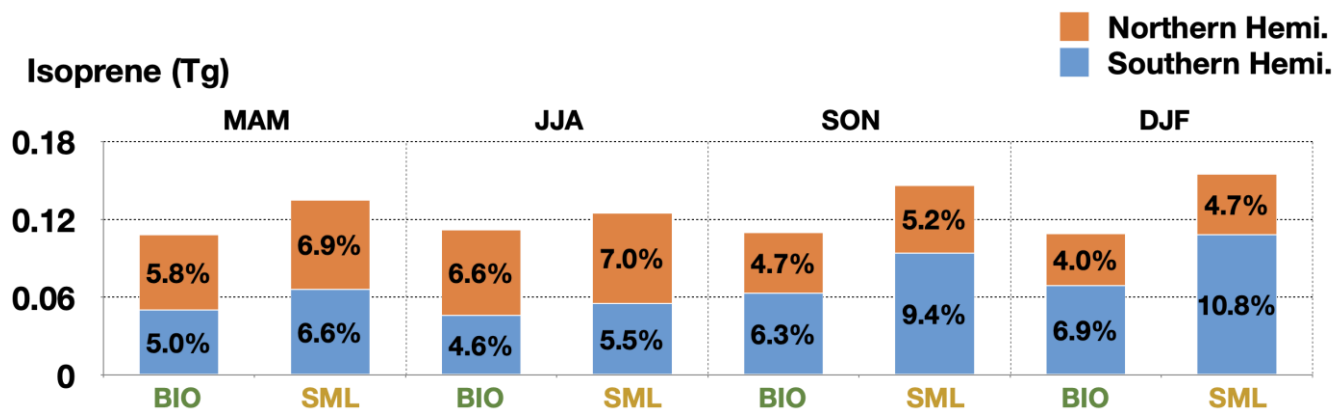
Figure 5: Seasonal variation of the contribution of BIO and SML emissions from two hemispheres to annual global emissions for the period 2001-2020.

530

Based on the datasets, we can find distinct spatial characteristics in marine isoprene emissions at a global scale, revealing specific patterns in annual emissions (Fig. 6). The BIO emissions are closely linked to chlorophyll concentration, exhibiting a similar spatial pattern to marine chlorophyll (Fig. 6a, 6c). Regions such as coastal areas, convergence zones, and upwelling areas (e.g., East China Sea, tropical Pacific, Offshore Peru) exhibit high BIO

535   emissions due to the presence of elevated chlorophyll concentrations and abundant nutrients. These conditions may arise from anthropogenic eutrophication in coastal areas or the natural flow of ocean current systems (Dai et al., 2023). The emission rates in coastal areas is significantly larger than the remote ocean by several orders of magnitude. In the twenty-year period, the mean isoprene BIO emission per unit area in the coastal ocean (East Asia, 110E-130E, 40N-20N) is 0.273 $\mu g \cdot m^{-2} \cdot h^{-1}$, while the average emission is 0.076 $\mu g \cdot m^{-2} \cdot h^{-1}$ in remote ocean area

540   (Subtropic Pacific, 180W-120W, 20S-30S). The global average BIO emission per unit area is 0.141 $\mu g \cdot m^{-2} \cdot h^{-1}$. However, the emission from the remote ocean still dominates global marine isoprene emissions due to the vast surface area of remote ocean regions. Additionally, there is evidence of an increased frequency of potential phytoplankton bloom events, particularly in coastal regions and the Southern Ocean, over the past two decades (Dai et al., 2023). The spatial distribution of SML emissions is more uniform than that of BIO emissions and is

545   limited in range. Indirect use of chlorophyll data contributed to this characterization, in which the surfactant concentrations were determined from chlorophyll and divided into three bins. Therefore, SML emissions are insensitive to chlorophyll concentration, which results in a different spatial pattern of SML emissions and chlorophyll. SML emissions contribute relatively larger isoprene emission in the subtropic remote ocean. In these regions, SML emissions are dominated by radiation and windspeed. This relationship is further discussed in Sect.

550   4.2.
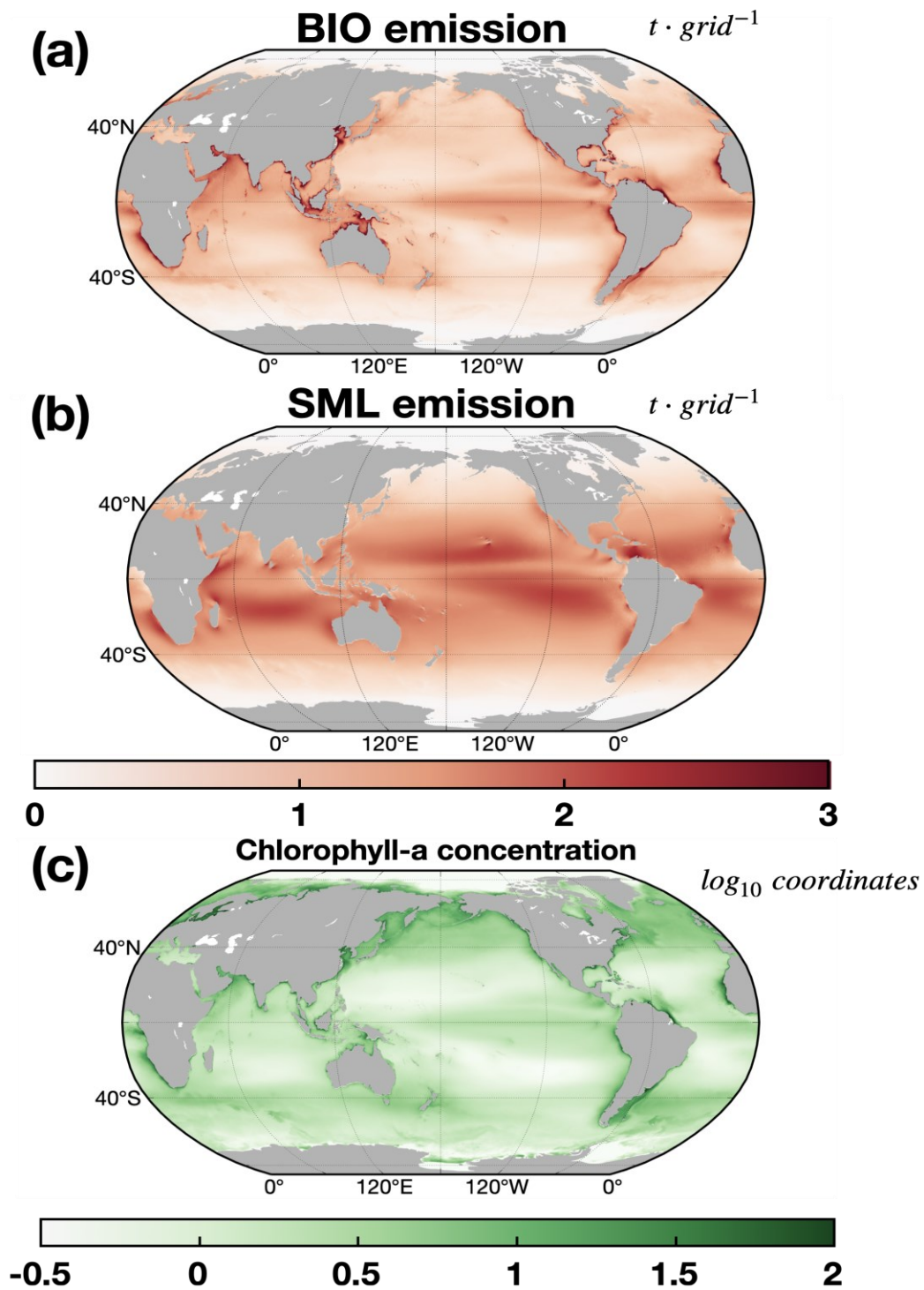
Figure 6: Mean annual BIO emissions (a), annual SML emissions (b) (unit in t), and annual Chlorophyll-a concentration (c) (in log10 coordinates) for twenty years.

The annual average global marine isoprene BIO and SML emissions exhibit a slight decreasing trend over the last twenty years (Fig. 7b). However, the emission trends vary significantly among different ocean regions. The annual emission from Pacific (49.5 %) and Indian Ocean (22.2 %) contributes 71.7 % to the global isoprene emission and emissions in both regions were decreasing in the last twenty years (Fig. 7a). In contrast, the Arctic Ocean shows an increasing trend in annual emissions, although its contribution to the global marine isoprene emission is only 1.2 % (Fig. 7a, 7c). This increasing trend in the Arctic ocean was further analysed using sea ice concentration and chlorophyll concentration data. We find that shrinkage of the sea ice extent and reduce of the sea ice concentration in recent decades lead to increase in both emission area and period in boreal summer. Additionally, recent research suggests that along with the ice-free area lasting longer, the novel fall phytoplankton blooms are more likely to happen (Ardyna et al., 2014). The bloom events may contribute to the increasing of isoprene emission potentially.

The emissions in the low latitude ocean are most important over the global marine isoprene emission attributed by the intense radiation, and high concentration of chlorophyll relative to subtropical remote ocean, which account for 36.7 % of global marine isoprene emission. "This trend is controlled by the tropical air-sea system potentially. Our former investigation suggest that the ENSO influence the tropical Pacific isoprene emission significantly when the ENSO is at its strong positive or negative phase. In the strong positive phase, the tropical west wind is strengthened, which leads to the warm water accumulate in the tropical Pacific. This process makes the increase of sea surface temperature in the tropic Pacific, which further weakens the isoprene emission in this area.". The SML emission in low latitudes was decreased by 5.6 % per year while the BIO emission was decreased by 3.0 % per year over the twenty-year period (Fig. 7a, 7b). In addition, the SML emission Atlantic is also with a decreasing trend, while the BIO emission has no specific trend in the twenty-year period.

575
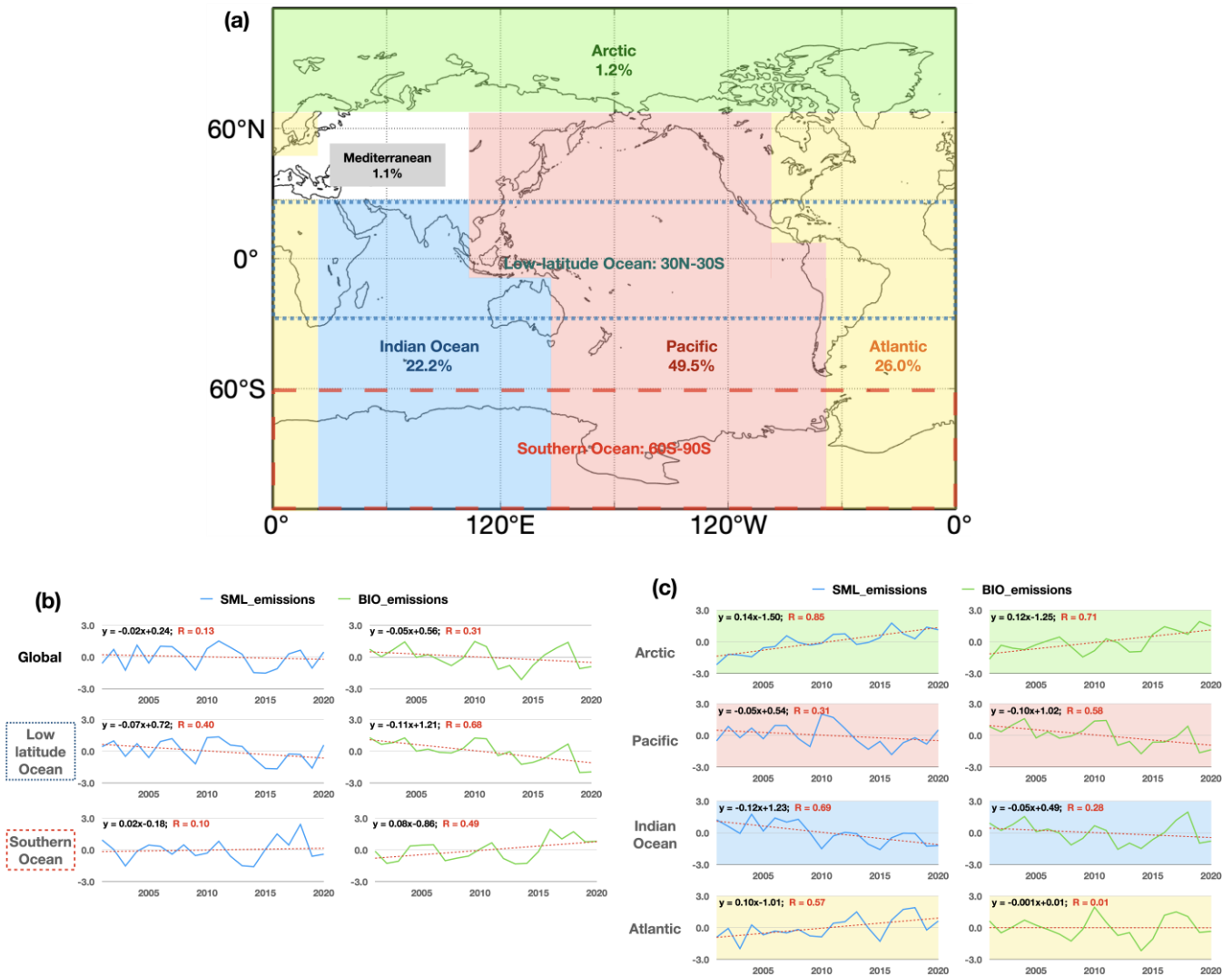
Figure 7: Twenty-year mean contributions of annual isoprene emissions from different ocean regions to global annual emissions (a) and standardized trends of two types of annual isoprene emissions in different ocean regions (b, c).

4.2 Influence of marine and meteorological factors

580 The variations of isoprene emissions are primarily influenced by marine and meteorological conditions, both directly and indirectly. The effects of four dominant factors including 10-meter windspeed, surface downward solar radiation, sea surface temperature and marine chlorophyll concentration, were examined by correlating them with BIO and SML emissions (Fig. 8). Chlorophyll concentration is considered a factor that quantifies nutrient levels and phytoplankton activities, which also was used to determine the surfactant content in the sea surface microlayer.

585 Globally, chlorophyll concentration has a significant positive correlation (r = 0.67, p ≤ 0.05) with BIO emissions (Fig. 8g). However, chlorophyll concentration shows positive correlation with SML emissions in the polar, subpolar and tropical regions, while negative correlation in the subtropical region, suggesting that other critical factors control SML emissions in these areas (Fig. 8h). Surface solar radiation downward is another important factor influencing both BIO emissions and SML emissions. There is a globally positive correlation between surface

590 solar radiation downward and SML emissions (Fig. 8d), with a significant coefficient of r = 0.62 (p ≤ 0.05) in the global average, while positive correlations with BIO emissions are only found on mid and high latitudes beyond 40°N and 40°S (Fig. 8c). Sea surface temperature and 10-meter windspeed have less impact on BIO and SML emissions compare to the other two factors in most open ocean areas. Large number of grid cells with weak correlations (|r| ≤ 0.4) and correlations that did not pass our significance test (p > 0.05) for sea surface temperature

595 and 10-meter windspeed with BIO and SML emissions are shown in Fig. 8 (Fig. 8a, 8b, 8e, 8f). These two physical factors affect marine isoprene emissions indirectly by altering the air-sea exchange processes, and show contrasting correlations, especially in tropical ocean (Fig. 8a, 8b, 8e, 8f), where BVOCs emission is determined by local atmosphere and ocean conditions (Xu et al., 2016). The wind mainly contributed to the SML emission. First, it determined the surfactant coverage on the ocean surface. A wind threshold of 13 m·s-1 is used to restrict the extent

600 of sea micro-layer. Besides, the wind is input data for exchange velocity in sea micro-layer, which is directly correspond to the cube of wind. This cubic relationship makes the SML emissions are positive correlated to the wind. In Fig. 8b, wind speed shows positive correlations with SML emissions in the low-latitude and several coastal regions, while negative correlations appear in high-latitude. We think this spatial difference is caused by the wind threshold. In the low-latitude and coastal regions, the wind keeps a relative low level according to the threshold.

605 Therefore, when the wind increases in these areas, the SML emissions will follow accordingly. On the country, the wind increases in high-latitude leads to more grid cells with the windspeed beyond the limit, which result in no emissions in these areas. Finally, it turns out a negative relationship.

The sea surface temperature was not directly used in both BIO and SML emissions calculations. In fact, the SST affects the marine productivity by modifying the biological activity of phytoplankton. However, previous study

610 proved that the SST only dominant the phytoplankton productivity when the nutrient conditions is not limited. This conclusion can be derived from Fig. 8c and 8d, which the subtropical remote ocean is showed with no correlations. On the other hand, phytoplankton has a suitable temperature range for its growth and metabolic processes. It explained the positive relationship appears in the tropical ocean with higher SST, while negative correlation is in the high latitude ocean which is colder. The variations of marine and meteorological factors are all the result of

615 variation of air-sea system, suggesting that the variability of large-scale air-sea systems may contribute to the

variability in marine isoprene emissions (Abbatt et al., 2019; Hackenberg et al., 2017; Xu et al., 2016; Zhang and Gu, 2022). The air-sea system plays a leading role in the marine isoprene emission. The air-sea system such as MJO, ENSO and IOD may have potential influence on the marine isoprene emissions. Large-scale air-sea system is a combination of atmospheric and oceanic systems with their characteristics, mechanisms and interactions in a large spatial range. These systems dominate the dynamic processes as well as marine and meteorological factors with their specific patterns in the global scale, especially in the tropical and subtropical area (eg. ENSO, MJO), where important isoprene emissions with explicit variations and spatial patterns are found. With the adequate understanding of these air-sea systems, we can better comprehend the mechanisms and characteristics of marine isoprene emissions.
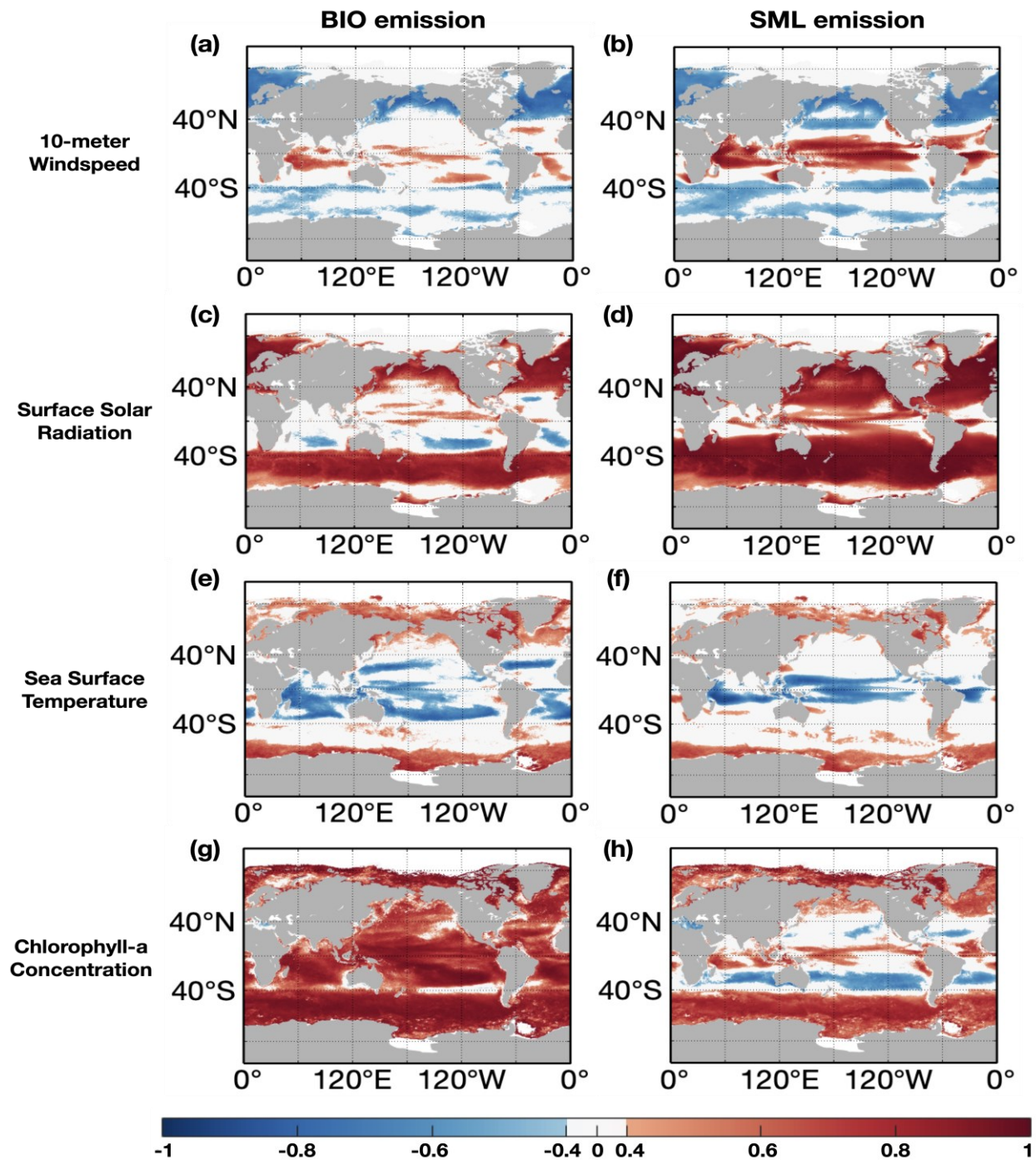
Figure 8: Correlation coefficients of monthly factors including 10-meter windspeed (a, b) , surface solar radiation downward (c, d), sea surface temperature (e, f) and chlorophyll concentration (g, h) with monthly BIO emissions (a, c, e, g) and with monthly SML emissions (b, d, f, h). Note that the grids where the absolute values of correlation coefficients are above 0.4 (P ≤ 0.05) are filled with colours.

625

4.3 Potential effects of the air-sea system

In order to locate and investigate the potential impact of air-sea systems on isoprene emissions, the multiple variables empirical orthogonal function (MVEOF) was employed to examine the spatial pattern of temporal variation in BIO and SML isoprene emissions (Fig. 9). From a global perspective, the leading MVEOF principal component (39.88 % explained variance) reveals a seasonal periodicity in both types of emissions, with a symmetrical pattern between the two hemispheres (Fig. 9a-d). In addition, the other principal components do not exhibit any distinct or meaningful spatial patterns. The same analysis method was used to identify the leading potential pattern for the tropical and subtropical regions (30° N-30° S) (Fig. 9e-f). In this case, two leading EOF modes are presented, with the sum of explained variances of 37.76 %. The first mode suggests that BIO and SML emissions have different spatial pattern, in which the BIO emissions show potential opposite patterns between the coastal and remote ocean regions. The second leading mode reveals a distinct signal in the Indian Ocean, characterized by a symmetric pattern resembling the Indian Ocean Dipole (IOD), which is a dominant quasi-periodic variation in sea surface temperature in the Indian Ocean. For SML emissions, the first mode shows an El Niño-Southern Oscillation (ENSO)-like spatial pattern in the tropical Pacific. This suggests a connection between annual and seasonal variations in isoprene emissions and the large-scale air-sea system variability. It is likely that marine isoprene emissions are influenced by air-sea interactions, including ENSO and other climate patterns at various scales. Previous studies have also found increased marine DMS emissions in the tropical Pacific during La Niña events due to anomalies in sea surface winds (Xu et al., 2016).
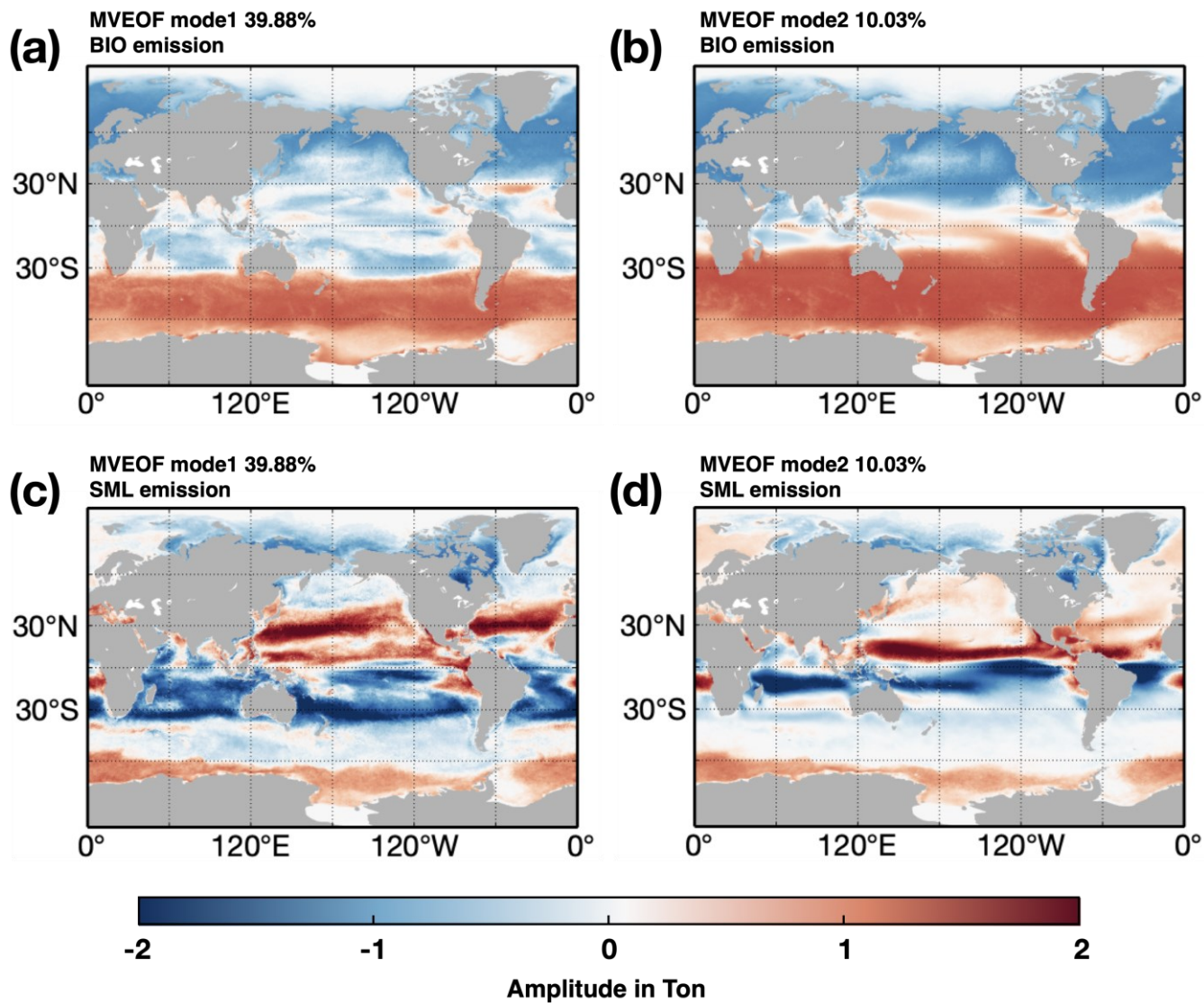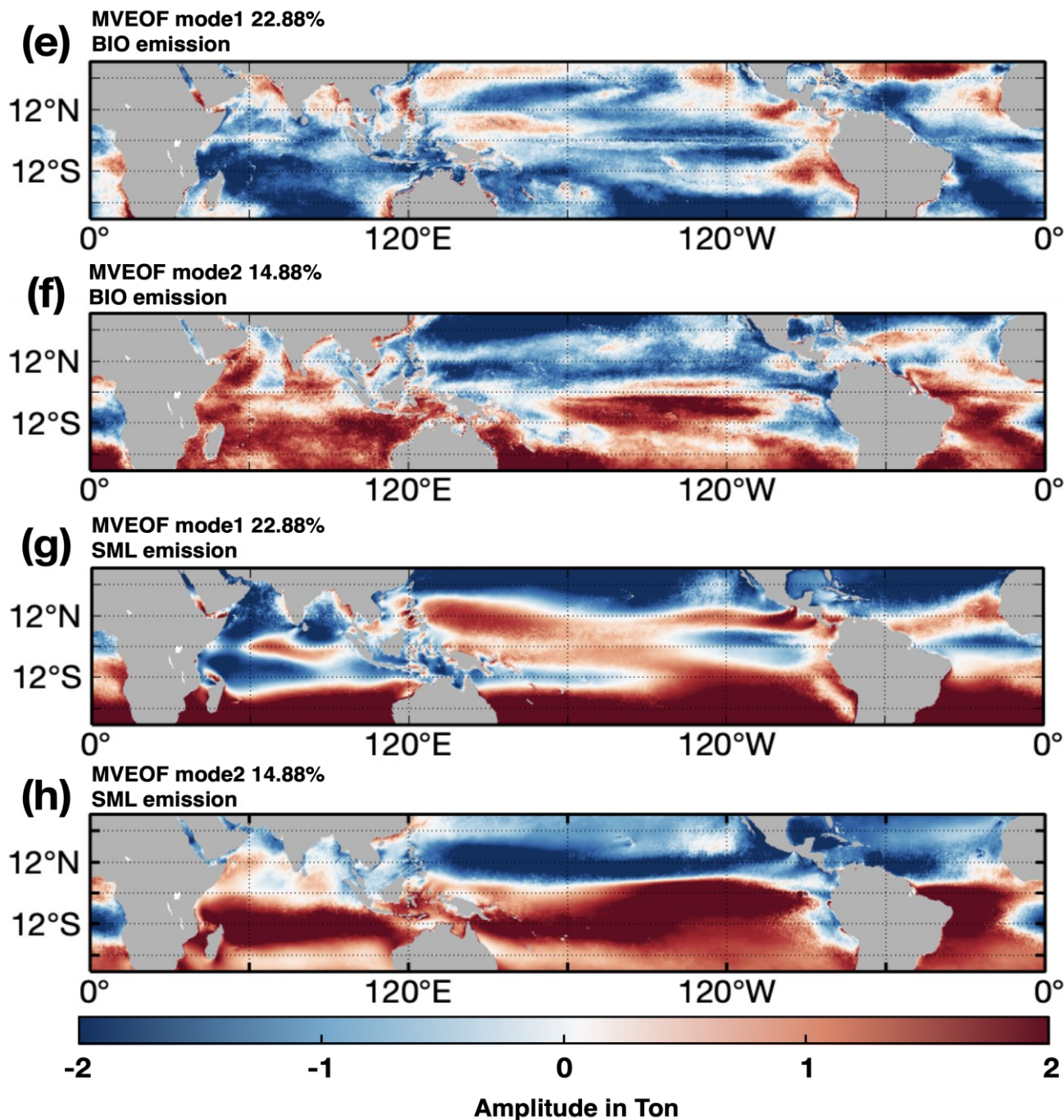
650

Figure 9: MVEOF results for global emission (a-d) and low latitude (30° N-30° S) emission (e-h). a-b and e-f is the first two mode of BIO emission, c-d and g-h is the first two mode of SML emission. In the global extent, the explained variances for leading two modes are 39.88 % and 10.03 %. In the low latitudes, the explained variances for leading two modes are 22.88 % and 14.88 %. The amplitudes are in tons.

655 To further investigate the periodic changes in isoprene emissions and identify corresponding air-sea systems with similar cycles, wavelet analysis was applied to the monthly data. This analysis allowed us to identify significant periods in different regions. At the global scale, interannual variability is the most common and prominent for both BIO emissions and SML emissions (Fig. 10). This annual signal is largely influenced by the solar radiation cycle. Besides, a half-year period was derived from the mid-latitude and tropical SML emissions. The same period was

660 also observed for BIO emissions in mid-latitude ocean. Furthermore, a significant intraseasonal period was found in the tropical Indian Ocean and the tropical Pacific (Fig. 10c). This period, shorter than a season (0.25 years), occurs almost every year and is believed to be associated with the Madden-Julian Oscillation (MJO). The MJO is a dominant component of tropical intraseasonal variability and is associated with the large-scale signal of deep convection, which strongly affects precipitation and radiation in the tropical ocean area. The periodic information

665 is a potential indicator to find and link emission variations and driver changes. These identified periods demonstrate the potential relationships between marine isoprene emissions and variations in the air-sea system.
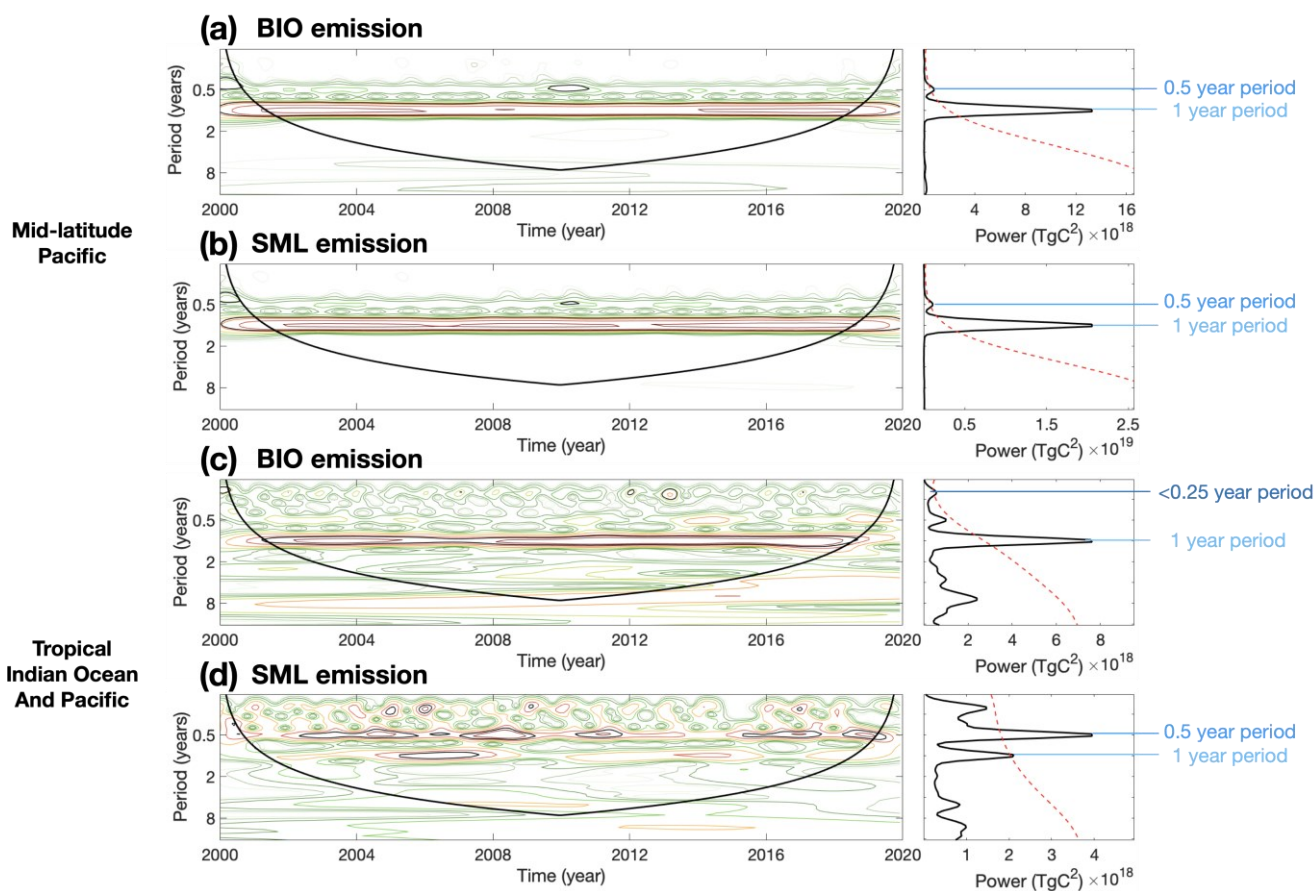
Figure 10: Wavelet power spectrum and time averaged wavelet spectrum of BIO emission (a and c) and SML emission (b and d) of mid latitude Pacific (a-b) and tropical Indian Ocean and Pacific (c-d). The black irregular closed contours in the left column represent periods which the significance level is greater than 95%. The symmetrical black solid curve in the left column is cone of influence. Period signals above this curve is available. Red dash lines in the right column represents the 95% significance level. The peaks of the black curves in the right row over the red dash lines is of 95% significance in the twenty-year period average.

5 Data availability

Hourly global marine isoprene BIO and SML emission dataset at a spatial resolution of 0.25°×0.25° from 2001 to 2020 can be accessed directly through: http://dx.doi.org/10.11888/Atmos.tpdc.300521 (Cui and Zhu, 2023).

6 Summary

680   In this work, a new marine isoprene emission module was built to generate a dataset of marine isoprene emissions with improved spatial and temporal resolution. This was achieved by incorporating comprehensive parameterized solutions based on remote sensing data on ocean chlorophyll concentration and reanalysis of climate data. The module considers separate parameterizations for BIO emissions and SML emissions, taking into account different physical processes. Our module estimate the total global marine isoprene emissions to be 1.097 Tg·yr^{-1} on average

685   over a twenty-year period, with 0.481 Tg·yr^{-1} attributed to BIO emissions and 0.616 Tg·yr^{-1} to SML emissions. To validate our results, several observations of marine isoprene concentrations and emission fluxes were collected for comparison with our results. These comparisons demonstrate the reasonableness and consistency of our data.

Using the hourly data, we conducted a detailed analysis of the spatial and temporal distributions of marine isoprene emissions, including their trends and periodic characteristics. On a global scale, significant disparities and

690   variations in emissions between the Southern Hemisphere and the Northern Hemisphere have been observed, displaying distinct seasonal patterns. The emissions from the Southern Hemisphere play a crucial role, particularly during the boreal winter, while the emissions in the Northern Hemisphere amount to only half of those in the Southern Hemisphere. Isoprene emissions are unevenly distributed across various ocean regions. Eutrophic ocean areas, such as coastal regions and eastern boundary current systems, consistently demonstrate higher marine

695   isoprene emissions compared to remote oligotrophic ocean areas, often by orders of magnitude. We identified a slight decreasing trend in global annual isoprene emissions over the 2001-2020 period, which is dominated by a significant decrease trend at low latitudes. Through wavelet analysis, multiple significant periods of isoprene emissions are found, including annual, semi-annual and intraseasonal periods in different ocean regions. Several periodic and quasi-periodic signals appear in the tropical and subtropical Indian Ocean and Pacific. These findings

700   indicate that air-sea systems drive isoprene emissions, particularly in the tropical and subtropical Indian Ocean and Pacific regions. These quasi-periodic patterns and their relationships with emissions provide valuable insights for refining existing methods and improving the reliability of isoprene emission estimations. They also help bridge the gap and lessen discrepancies between observations and model calculations.

Author Contribution

705   JZ conceived the research; LC and JZ designed the module, performed emission module runs, created the emission dataset and analyzed the data. YX contributed to the preparation of module input and data processing; YX, WH,

LS, YW, CZ and PF joined the discussion of the research and offered advice; LC wrote the first draft of the manuscript; JZ and LC revised the manuscript before submission with contributions from all co-authors.

Competing interests

710 The authors have declared that they have no conflict of interest.

Acknowledgement

The monthly normalized water-leaving radiance data at 410 nm for the period of 2012-2020 were provided by NOAA's Center for Satellite Applications and Research (STAR) and the CoastWatch program.

Financial support

715 This research has been supported by supported by National Key R&D Plan(Grant No.2022YFF0803000) and National Natural Science Foundation of China (Grant No. 42177082).

References

Abbatt, J. P. D., Leaitch, W. R., Aliabadi, A. A., Bertram, A. K., Blanchet, J. P., Boivin-Rioux, A., Bozem, H., Burkart, J.,
Chang, R. Y. W., Charette, J., Chaubey, J. P., Christensen, R. J., Cirisan, A., Collins, D. B., Croft, B., Dionne, J., Evans,
720 G. J., Fletcher, C. G., Gali, M., Ghahreman, R., Girard, E., Gong, W. M., Gosselin, M., Gourdal, M., Hanna, S. J.,
Hayashida, H., Herber, A. B., Hesaraki, S., Hoor, P., Huang, L., Hussherr, R., Irish, V. E., Keita, S. A., Kodros, J. K.,
Kollner, F., Kolonjari, F., Kunkel, D., Ladino, L. A., Law, K., Levasseur, M., Libois, Q., Liggio, J., Lizotte, M.,
Macdonald, K. M., Mahmood, R., Martin, R. V., Mason, R. H., Miller, L. A., Moravek, A., Mortenson, E., Mungall, E.
L., Murphy, J. G., Namazi, M., Norman, A. L., O'Neill, N. T., Pierce, J. R., Russell, L. M., Schneider, J., Schulz, H.,
725 Sharma, S., Si, M., Staebler, R. M., Steiner, N. S., Thomas, J. L., von Salzen, K., Wentzell, J. J. B., Willis, M. D.,
Wentworth, G. R., Xu, J. W., and Yakobi-Hancock, J. D.: Overview paper: New insights into aerosol and climate in the
Arctic, Atmos Chem Phys, 19, 2527-2560, https://doi.org/10.5194/acp-19-2527-2019, 2019.
Alvain, S., Moulin, C., Dandonneau, Y., and Breon, F. M.: Remote sensing of phytoplankton groups in case 1 waters from
global SeaWiFS imagery, Deep-Sea Res Pt I, 52, 1989-2004, https://doi.org/10.1016/j.dsr.2005.06.015, 2005.
730 Alvain, S., Moulin, C., Dandonneau, Y., and Loisel, H.: Seasonal distribution and succession of dominant phytoplankton
groups in the global ocean: A satellite view, Global Biogeochem Cy, 22, Artn Gb3001
https://doi.org/10.1029/2007gb003154, 2008.

Ardyna, M., Babin, M., Gosselin, M., Devred, E., Rainville, L., & Tremblay, J. E. (2014). Recent Arctic Ocean sea ice loss triggers novel fall phytoplankton blooms. Geophysical Research Letters, 41(17), 6207-6212. https://doi.org/10.1002/2014gl061047

Arnold, S. R., Spracklen, D. V., Williams, J., Yassaa, N., Sciare, J., Bonsang, B., Gros, V., Peeken, I., Lewis, A. C., Alvain, S., and Moulin, C.: Evaluation of the global oceanic isoprene source and its impacts on marine organic carbon aerosol, Atmos Chem Phys, 9, 1253-1262, https://doi.org/10.5194/acp-9-1253-2009, 2009.

Booge, D., Schlundt, C., Bracher, A., Endres, S., Zancker, B., and Marandino, C. A.: Marine isoprene production and consumption in the mixed layer of the surface ocean - a field study over two oceanic regions, Biogeosciences, 15, 649-667, https://doi.org/10.5194/bg-15-649-2018, 2018.

Bonsang, B., Polle, C., & Lambert, G. (1992). Evidence for marine production of isoprene. Geophysical Research Letters, 19(11), 1129-1132. https://doi.org/10.1029/92GL00083, 1992

Booge, D., Marandino, C. A., Schlundt, C., Palmer, P. I., Schlundt, M., Atlas, E. L., Bracher, A., Saltzman, E. S., and Wallace, D. W. R.: Can simple models predict large-scale surface ocean isoprene concentrations? Atmos Chem Phys, 16, 11807-11821, https://doi.org/10.5194/acp-16-11807-2016, 2016.

Brüggemann, M., Hayeck, N., and George, C.: Interfacial photochemistry at the ocean surface is a global source of organic vapors and aerosols, Nat Commun, 9, ARTN 2101 https://doi.org/10.1038/s41467-018-04528-7, 2018.

Brüggemann, M., Hayeck, N., Bonnineau, C., Pesce, S., Alpert, P. A., Perrier, S., Zuth, C., Hoffmann, T., Chen, J. M., and George, C.: Interfacial photochemistry of biogenic surfactants: a major source of abiotic volatile organic compounds, Faraday Discuss, 200, 59-74, https://doi.org/10.1039/c7fd00022g, 2017.

Carslaw, K. S., Boucher, O., Spracklen, D. V., Mann, G. W., Rae, J. G. L., Woodward, S., and Kulmala, M.: A review of natural aerosol interactions and feedbacks within the Earth system, Atmos Chem Phys, 10, 1701-1737, https://doi.org/10.5194/acp-10-1701-2010, 2010.

Ciuraru, R., Fine, L., van Pinxteren, M., D'Anna, B., Herrmann, H., and George, C.: Unravelling New Processes at Interfaces: Photochemical Isoprene Production at the Sea Surface, Environ Sci Technol, 49, 13199-13205, https://doi.org/10.1021/acs.est.5b02388, 2015a.

Ciuraru, R., Fine, L., van Pinxteren, M., D'Anna, B., Herrmann, H., and George, C.: Photosensitized production of functionalized and unsaturated organic compounds at the air-sea interface, Sci Rep-Uk, 5, ARTN 12741 https://doi.org/10.1038/srep12741, 2015b.

Claeys, M., Wang, W., Ion, A. C., Kourtchev, I., Gelencser, A., and Maenhaut, W.: Formation of secondary organic aerosols from isoprene and its gas-phase oxidation products through reaction with hydrogen peroxide, Atmos Environ, 38, 4093-4098, https://doi.org/10.1016/j.atmosenv.2004.06.001, 2004.

Conte, L., Szopa, S., Aumont, O., Gros, V., and Bopp, L.: Sources and Sinks of Isoprene in the Global Open Ocean: Simulated Patterns and Emissions to the Atmosphere, J Geophys Res-Oceans, 125, ARTN e2019JC015946 https://doi.org/10.1029/2019JC015946, 2020.

Cui, L., Zhu, J.: Global marine isoprene emission data set (2001-2020), National Tibetan Plateau Data Center [data set], http://dx.doi.org/10.11888/Atmos.tpdc.300521, 2023.

Dai, Y., Yang, S., Zhao, D., Hu, C., Xu, W., Anderson, D. M., Li, Y., Song, X.-P., Boyce, D. G., Gibson, L., Zheng, C., and Feng, L.: Coastal phytoplankton blooms expand and intensify in the 21st century, Nature, 615, 280-284, https://doi.org/10.1038/s41586-023-05760-y, 2023.

Dani, K. G. S. and Loreto, F.: Trade-Off Between Dimethyl Sulfide and Isoprene Emissions from Marine Phytoplankton, Trends Plant Sci, 22, 361-372, https://doi.org/10.1016/j.tplants.2017.01.006, 2017.

Gantt, B., Meskhidze, N., and Kamykowski, D.: A new physically-based quantification of marine isoprene and primary organic aerosol emissions, Atmos Chem Phys, 9, 4915-4927, https://doi.org/10.5194/acp-9-4915-2009, 2009.

Gantt, B., Xu, J., Meskhidze, N., Zhang, Y., Nenes, A., Ghan, S. J., Liu, X., Easter, R., and Zaveri, R.: Global distribution and climate forcing of marine organic aerosol - Part 2: Effects on cloud properties and radiative forcing, Atmos Chem Phys, 12, 6555-6563, https://doi.org/10.5194/acp-12-6555-2012, 2012.

Guenther, A., Karl, T., Harley, P., Wiedinmyer, C., Palmer, P. I., and Geron, C.: Estimates of global terrestrial isoprene emissions using MEGAN (Model of Emissions of Gases and Aerosols from Nature), Atmos Chem Phys, 6, 3181-3210, https://doi.org/10.5194/acp-6-3181-2006, 2006.

Guenther, A. B., Jiang, X., Heald, C. L., Sakulyanontvittaya, T., Duhl, T., Emmons, L. K., and Wang, X.: The Model of Emissions of Gases and Aerosols from Nature version 2.1 (MEGAN2.1): an extended and updated framework for modeling biogenic emissions, Geosci Model Dev, 5, 1471-1492, https://doi.org/10.5194/gmd-5-1471-2012, 2012.

Guo, S. J., Feng, Y. Y., Wang, L., Dai, M. H., Liu, Z. L., Bai, Y., and Sun, J.: Seasonal variation in the phytoplankton community of a continental-shelf sea: the East China Sea, Mar Ecol Prog Ser, 516, 103-126, https://doi.org/10.3354/meps10952, 2014.

Hackenberg, S. C., Andrews, S. J., Airs, R., Arnold, S. R., Bouman, H. A., Brewin, R. J. W., Chance, R. J., Cummings, D., Dall'Olmo, G., Lewis, A. C., Minaeian, J. K., Reifel, K. M., Small, A., Tarran, G. A., Tilstone, G. H., and Carpenter, L. J.: Potential controls of isoprene in the surface ocean, Global Biogeochem Cy, 31, 644-662, https://doi.org/10.1002/2016gb005531, 2017.

Hersbach, H., Bell, B., Berrisford, P., Biavati, G., Horányi, A., Muñoz Sabater, J., Nicolas, J., Peubey, C., Radu, R., Rozum, I., Schepers, D., Simmons, A., Soci, C., Dee, D., Thépaut, J-N. (2023): ERA5 hourly data on single levels from 1940 to present. Copernicus Climate Change Service (C3S) Climate Data Store (CDS), https://doi.org/10.24381/cds.adbb2d47, 2023.

Kameyama, S., Yoshida, S., Tanimoto, H., Inomata, S., Suzuki, K., and Yoshikawa-Inoue, H.: High-resolution observations of dissolved isoprene in surface seawater in the Southern Ocean during austral summer 2010-2011, J Oceanogr, 70, 225-239, https://doi.org/10.1007/s10872-014-0226-8, 2014.

Kim, M. J., Novak, G. A., Zoerb, M. C., Yang, M. X., Blomquist, B. W., Huebert, B. J., Cappa, C. D., and Bertram, T. H.:
800   Air-Sea exchange of biogenic volatile organic compounds and the impact on aerosol particle size distributions, Geophys Res Lett, 44, 3887-3896, https://doi.org/10.1002/2017gl072975, 2017.

Li, J. L., Kameyama, S., and Yang, G. P.: In-situ measurement of trace isoprene and dimethyl sulfide in seawater and oceanic atmosphere based on room temperature adsorption-thermal desorption, Mar Chem, 222, ARTN 103787 https://doi.org/10.1016/j.marchem.2020.103787, 2020.

805   Li, J. L., Zhang, H. H., and Yang, G. P.: Distribution and sea-to-air flux of isoprene in the East China Sea and the South Yellow Sea during summer, Chemosphere, 178, 291-300, https://doi.org/10.1016/j.chemosphere.2017.03.037, 2017.

Li, J. L., Zhai, X., Zhang, H. H., and Yang, G. P.: Temporal variations in the distribution and sea-to-air flux of marine isoprene in the East China Sea, Atmos Environ, 187, 131-143, https://doi.org/10.1016/j.atmosenv.2018.05.054, 2018.

Li, J. L., Zhai, X., Ma, Z., Zhang, H. H., and Yang, G. P.: Spatial distributions and sea-to-air fluxes of non-methane
810   hydrocarbons in the atmosphere and seawater of the Western Pacific Ocean, Sci Total Environ, 672, 491-501, https://doi.org/10.1016/j.scitotenv.2019.04.019, 2019.

Liu, X., Xiao, W. P., Landry, M. R., Chiang, K. P., Wang, L., and Huang, B. Q.: Responses of Phytoplankton Communities to Environmental Variability in the East China Sea, Ecosystems, 19, 832-849, https://doi.org/10.1007/s10021-016-9970-5, 2016.

815   Luo, G. and Yu, F.: A numerical evaluation of global oceanic emissions of alpha-pinene and isoprene, Atmos Chem Phys, 10, 2007-2015, https://doi.org/10.5194/acp-10-2007-2010, 2010.

Matsunaga, S., Mochida, M., Saito, T., and Kawamura, K.: In situ measurement of isoprene in the marine air and surface seawater from the western North Pacific, Atmos Environ, 36, 6051-6057, Pii S1352-2310(02)00657-X https://doi.org/10.1016/S1352-2310(02)00657-X, 2002.

820   McGillis, W. R., Edson, J. B., Zappa, C. J., Ware, J. D., McKenna, S. P., Terray, E. A., Hare, J. E., Fairall, C. W., Drennan, W., Donelan, M., DeGrandpre, M. D., Wanninkhof, R., and Feely, R. A.: Air-sea CO2 exchange in the equatorial Pacific, J Geophys Res-Oceans, 109, Artn C08s02 https://doi.org/10.1029/2003jc002256, 2004.

Meskhidze, N., Xu, J., Gantt, B., Zhang, Y., Nenes, A., Ghan, S. J., Liu, X., Easter, R., and Zaveri, R.: Global distribution and climate forcing of marine organic aerosol: 1. Model improvements and evaluation, Atmos Chem Phys, 11, 11689-11705,
825   https://doi.org/10.5194/acp-11-11689-2011, 2011.

Myriokefalitakis, S., Vignati, E., Tsigaridis, K., Papadimas, C., Sciare, J., Mihalopoulos, N., Facchini, M. C., Rinaldi, M., Dentener, F. J., Ceburnis, D., Hatzianastasiou, N., O'Dowd, C. D., van Weele, M., and Kanakidou, M.: Global Modeling of the Oceanic Source of Organic Aerosols, Adv Meteorol, 2010, Artn 939171 https://doi.org/10.1155/2010/939171, 2010.

NASA Goddard Space Flight Center, Ocean Ecology Laboratory, Ocean Biology Processing Group. Moderate-resolution
830   Imaging Spectroradiometer (MODIS) Terra Chlorophyll Data; 2022 Reprocessing. NASA OB.DAAC, Greenbelt, MD, USA. https://doi.org/10.5067/TERRA/MODIS/L3M/CHL/2022, 2023.

NASA Goddard Space Flight Center, Ocean Ecology Laboratory, Ocean Biology Processing Group. Moderate-resolution Imaging Spectroradiometer (MODIS) Terra Downwelling Diffuse Attenuation Coefficient Data; 2022 Reprocessing. NASA OB.DAAC, Greenbelt, MD, USA. https://doi.org/10.5067/TERRA/MODIS/L3M/KD/2022, 2023.

835 Novak, G. A. and Bertram, T. H.: Reactive VOC Production from Photochemical and Heterogeneous Reactions Occurring at the Air-Ocean Interface, Accounts Chem Res, 53, 1014-1023, https://doi.org/10.1021/acs.accounts.0c00095, 2020.

Ooki, A., Nomura, D., Nishino, S., Kikuchi, T., and Yokouchi, Y.: A global-scale map of isoprene and volatile organic iodine in surface seawater of the Arctic, Northwest Pacific, Indian, and Southern Oceans, J Geophys Res-Oceans, 120, 4108-4128, https://doi.org/10.1002/2014jc010519, 2015.

840 Palmer, P. I. and Shaw, S. L.: Quantifying global marine isoprene fluxes using MODIS chlorophyll observations, Geophys Res Lett, 32, https://doi.org/10.1029/2005gl022592, 2005.

Phillips, D. P., Hopkins, F. E., Bell, T. G., Liss, P. S., Nightingale, P. D., Reeves, C. E., Wohl, C., and Yang, M. X.: Air-sea exchange of acetone, acetaldehyde, DMS and isoprene at a UK coastal site, Atmos Chem Phys, 21, 10111-10132, https://doi.org/10.5194/acp-21-10111-2021, 2021.

845 Rosenfeld, D., Andreae, M. O., Asmi, A., Chin, M., de Leeuw, G., Donovan, D. P., Kahn, R., Kinne, S., Kivekas, N., Kulmala, M., Lau, W., Schmidt, K. S., Suni, T., Wagner, T., Wild, M., and Quaas, J.: Global observations of aerosol-cloud-precipitation-climate interactions, Rev Geophys, 52, 750-808, https://doi.org/10.1002/2013RG000441, 2014.

Sabbaghzadeh, B., Upstill-Goddard, R. C., Beale, R., Pereira, R., and Nightingale, P. D.: The Atlantic Ocean surface microlayer from 50 degrees N to 50 degrees S is ubiquitously enriched in surfactants at wind speeds up to 13ms(-1),
850 Geophys Res Lett, 44, 2852-2858, https://doi.org/10.1002/2017gl072988, 2017.

Shaw, S. L., Chisholm, S. W., and Prinn, R. G.: Isoprene production by Prochlorococcus, a marine cyanobacterium, and other phytoplankton, Mar Chem, 80, 227-245, Pii S0304-4203(02)00101-9 https://doi.org/10.1016/S0304-4203(02)00101-9, 2003.

Shaw, S. L., Gantt, B., and Meskhidze, N.: Production and Emissions of Marine Isoprene and Monoterpenes: A Review, Adv
855 Meteorol, 2010, Artn 408696 https://doi.org/10.1155/2010/408696, 2010.

Simo, R., Cortes-Greus, P., Rodriguez-Ros, P., and Masdeu-Navarro, M.: Substantial loss of isoprene in the surface ocean due to chemical and biological consumption, Commun Earth Environ, 3, ARTN 20 https://doi.org/10.1038/s43247-022-00352-6, 2022.

Sinha, V., Williams, J., Meyerhofer, M., Riebesell, U., Paulino, A. I., and Larsen, A.: Air-sea fluxes of methanol, acetone,
860 acetaldehyde, isoprene and DMS from a Norwegian fjord following a phytoplankton bloom in a mesocosm experiment, Atmos Chem Phys, 7, 739-755, https://doi.org/10.5194/acp-7-739-2007, 2007.

Tripathi, N., Sahu, L. K., Singh, A., Yadav, R., and Karati, K. K.: High Levels of Isoprene in the Marine Boundary Layer of the Arabian Sea during Spring Inter-Monsoon: Role of Phytoplankton Blooms, Acs Earth Space Chem, 4, 583-590, https://doi.org/10.1021/acsearthspacechem.9b00325, 2020.

865 Uning, R., Latif, M. T., Abd Hamid, H. H., Nadzir, M. S. M., Khan, M. F., and Suratman, S.: Sea-to-Air Fluxes of Isoprene and Monoterpenes in the Coastal Upwelling Region of Peninsular Malaysia, Acs Earth Space Chem, 5, 3429-3436, https://doi.org/10.1021/acsearthspacechem.1c00270, 2021.

Wanninkhof, R.: Relationship between wind speed and gas exchange over the ocean revisited, Limnol Oceanogr-Meth, 12, 351-362, https://doi.org/10.4319/lom.2014.12.351, 2014.

870 Warneke, C., de Gouw, J. A., Goldan, P. D., Kuster, W. C., Williams, E. J., Lerner, B. M., Jakoubek, R., Brown, S. S., Stark, H., Aldener, M., Ravishankara, A. R., Roberts, J. M., Marchewka, M., Bertman, S., Sueper, D. T., McKeen, S. A., Meagher, J. F., & Fehsenfeld, F. C. (2004). Comparison of daytime and nighttime oxidation of biogenic and anthropogenic VOCs along the New England coast in summer during New England Air Quality Study 2002. Journal of Geophysical Research-Atmospheres, 109(D10). https://doi.org/Artn D10309

875 10.1029/2003jd004424

Wohl, C., Jones, A. E., Sturges, W. T., Nightingale, P. D., Else, B., Butterworth, B. J., and Yang, M. X.: Sea ice concentration impacts dissolved organic gases in the Canadian Arctic, Biogeosciences, 19, 1021-1045, https://doi.org/10.5194/bg-19-1021-2022, 2022.

Wohl, C., Li, Q. Y., Cuevas, C. A., Fernandez, R. P., Yang, M. X., Saiz-Lopez, A., and Simo, R.: Marine biogenic emissions

880 of benzene and toluene and their contribution to secondary organic aerosols over the polar oceans, Sci Adv, 9, ARTN eadd9031 https://doi.org/10.1126/sciadv.add9031, 2023.

Wurl, O., Wurl, E., Miller, L., Johnson, K., and Vagle, S.: Formation and global distribution of sea-surface microlayers, Biogeosciences, 8, 121-135, https://doi.org/10.5194/bg-8-121-2011, 2011.

Xu, L., Cameron-Smith, P., Russell, L. M., Ghan, S. J., Liu, Y., Elliott, S., Yang, Y., Lou, S., Lamjiri, M. A., and Manizza,

885 M.: DMS role in ENSO cycle in the tropics, J Geophys Res-Atmos, 121, 13537-13558, https://doi.org/10.1002/2016jd025333, 2016.

Yokouchi, Y., Li, H.-J., Machida, T., Aoki, S., and Akimoto, H.: Isoprene in the marine boundary layer (southeast Asian Sea, eastern Indian Ocean, and Southern Ocean): Comparison with dimethyl sulfide and bromoform, J. Geophys. Res., 104(D7), 8067– 8076, https://doi.org/10.1029/1998JD100013, 1999.

890 Yu, Z. J. and Li, Y.: Marine volatile organic compounds and their impacts on marine aerosol-A review, Sci Total Environ, 768, ARTN 145054 https://doi.org/10.1016/j.scitotenv.2021.145054, 2021.

Zhang, W. T. and Gu, D. S.: Geostationary satellite reveals increasing marine isoprene emissions in the center of the equatorial Pacific Ocean, Npj Clim Atmos Sci, 5, ARTN 83 https://doi.org/10.1038/s41612-022-00311-0, 2022.

Zhou, L., Booge, D., Zhang, M. M., and Marandino, C. A.: Winter season Southern Ocean distributions of climate-relevant

895 trace gases, Biogeosciences, 19, 5021-5040, https://doi.org/10.5194/bg-19-5021-2022, 2022.